Chapter 7   Tungsten Oxide Films

7.1.   Introduction

After Deb´s discovery [1] of the electrochromism of tungsten oxide (WO_3), it has been one of the most studied electrochromic (EC) materials [2, 3]. The characteristics of WO_3 films make them suitable for EC devices or windows [4, 5]. Depending on the deposition conditions and techniques, films may present considerably different structural, optical and electrical behaviors, and consequently different EC behaviors. The sputtering technique is the most widely investigated and large-scale deposition set available. Sputtered WO_3 films deposited on substrates are known to be amorphous or polycrystalline. Using tungsten (W) targets in direct current (d.c.) magnetron reactive sputtering, thin film properties can be improved by controlling the reactive gas atmosphere.

In addition, since mixed tungsten-molybdenum oxide has extremely broad absorption and physical properties in the colored state [6], some investigations of Molybdenum oxide (MoO_3) films were also done. MoO_3 has been known as a cathodic electrochromic material since 1974 [7]. Bulk crystals and films of MoO_3 have a structure consisting of corner-sharing chains of MoO_6 octahedra [8]. Its structure consists of an α – phase is similar to a WO_3 perovskite type (Section 7.2).

This chapter reports on the study of the deposition conditions and properties of WO_3 and Mo doped WO_3 films used for EC layers in a smart window. These films were characterized by using IR, UV-Vis-NIR, SEM, AFM, XRD and XPS. We will discuss the characterization of amorphous WO_3 films grown at RT and after a low temperature annealing process (25°-300°C). This low temperature process is necessary in order to fabricate smart EC windows or other functional multiplayer films.

7.2.   Structure of Tungsten Oxide Films

7.2.1.   General characteristics of WO₃ and transition metal oxides

An amorphous (α)–WO_3 film has a definite ionic and electronic conduction. It has large opened porous and it is constituted by clusters. The clusters are built from no more than 3-8 WO_6 –octahedra [9], linked together by corners or edges and in the complete structure of the film connected with one another by W-O-W bonds [10] or water bridges

[11]. The voids observed within the film are the result of random packing of the clusters and mostly give the open structure that is normally filled with molecular water taken from the air [10, 11]. The presence of water is necessary to stabilize the microcrystalline structure of an α–WO_3 film with the open pore structure. The ionic conduction of an α–WO_3 film is ensured by proton transport through channels or water bridges in pores, but the electronic conduction is done by the clusters linked together by W-O-W bonds.

The binary W-O system is rather complex with a large number of phases. The most stable WO_3 phase at room temperature has a monoclinic structure, but this phase transforms to an orthorhombic or a tetragonal phase at higher temperatures [12]. Many different structures of tungsten oxide clusters have been investigated [1]. The trioxide, WO_3 can crystallize in many polymorphs with various crystal structures [13].

Generally WO_3 and related electrochromic materials are divided into three main groups with regard to bulk crystalline structures. (i) Perovskite-like, such as WO_3, MoO_3, $SrTiO_3$; (ii) Rutile-like, TiO_2, MnO_2, VO_2, RuO_2, IrO_2 and RhO_2 ; (iii) Layer and block structures forming a somewhat undefined group, such as V_2O_5, Nb_2O_5. All the crystal structures have been studied by high resolution electron microscopy [6, 14]. A more detailed introduction will be presented in the following sections.

7.2.2. Perovskite-like Structure

The tungsten oxides consist of WO_6 –octahedra arranged in various sharing (corners, edges, planes) configurations. The main differences between the phases are shifts in the position of the W atoms within the octahedral, and variations in W-O bond lengths [15]. The simplest form with a general composition, WO_3 or $LiWO_3$, is the (defect) perovskite structure shown in Fig. 7-2-1a. As drawn, the W ions occupy the corners of a primitive unit cell, and O ions bisect the unit cell edges. The central atom is absent at the moment and will be denoted as Li or Na after the intercalated ions occupying symmetric positions. Each W ion is surrounded by six equidistant oxygen ions (Fig. 7-2-1a, part II). The stable monoclinic WO_3 can have a ReO_3-type structure (corner-sharing arrangement of octahehra). An infinite array of corner- sharing WO_6 –octahedra is formed like in Fig. 7-2-1b. These octahedras are in planes perpendicular to the [001] hexagonal axis and they form four membered rings in the *xy* or (001) plane. These layers are stacked in arrangement and are held together by weak van de Waal´s forces. The stacking of such planes along the z axis leads to the formation of tunnels between these octahedras (Fig. 7-2-1c). In the extended tunnel small ions can stay or move in

case of an exterior force. This may present the possibility of ionic transport and intercalation in the structure, and a mechanism for EC materials.
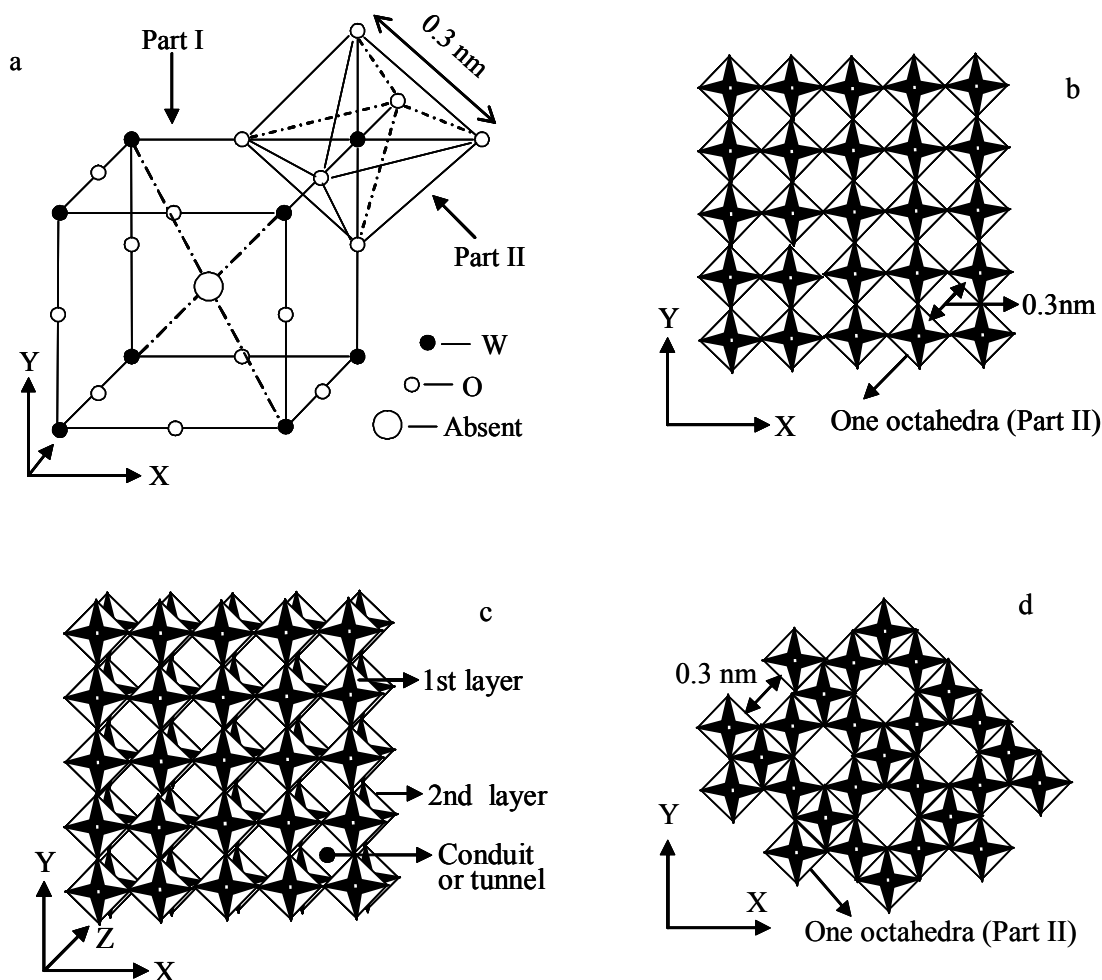

Fig.7-2-1. (a) Unit cell for the perovskite lattice (Part I) and octahedral symmetries (Part II) in the perovskite structure; (b) One layer of the monoclinic WO_3 structure in the corner-sharing arrangement of octahedra (ReO$_3$-type); (c) The monoclinic WO_3 structure (ReO$_3$-type); (d) One layer of the monoclinic WO_3 structure in the edge-sharing arrangement of octahedra.

7.2.3. Rutile-like Structure

The ideal rutile-like structure can be thought of as built from almost MeO_6 (Me=metal; O=oxygen) –octahedra units forming infinite edge-shared chains which can create vacant tunnels (Fig. 7-2-1d). Several oxygen deficient WO_{3-X} phases (Magneli phases) have been identified as the shear phase containing edge-shared octahedral [16]. In the substoichiometric tungsten oxides, $W_{18}O_{49}$ ($WO_{2.72}$) and $W_{20}O_{58}$ ($WO_{2.90}$), the shortage of oxygen is compensated by the formation of edge-sharing octahedra. The distances between the nearest W-W are widely distributed in these crystals [17]. Our

XRD results show the presence of $W_{20}O_{58}$ ($WO_{2.90}$) in Fig. 7-4-4 (Section 7.4). X-ray scattering is able to provide detailed structural information after Fourier transformations and computation of the scattering data. From Nanba et al. [17] the W-O nearest neighbor distance is ~0.2 nm. The W-W nearest neighbor distance is in the range 0.37 - 0.40 nm. The structure radial distribution 0.73 nm and all the above can be reconciled with a hexagonal structure and WO_6 –octahedra building blocks.

7.2.4. Tungsten oxide hydrates

Most of the above discussions are in ideal conditions. In fact tungsten oxide hydrates, $WO_3.nH_2O$, are common compounds made from sol-gel [18], even vacuum methods. They can be formed of layers built up by corner sharing (WO_6) octahedra, with water molecules between these layers. Its structure is similar to Fig. 7-2-1c. The formation of such layered structures from solute aqueous precursors is explained as follows. Hydrous oxides are precipitated upon the acidification of tungstate $(WO_4)^{2-}$, where neutral precursors $(H_2WO_4)^0$ are formed (Fig. 7-2-2a). Coordination expansion leads to the formation of six-fold coordinated W^{6+} via the nucleophilic addition of two water molecules (Fig.7-2-2a and 2b). However as the preferred coordination of W^{6+} is known to be mono-oxo (W=O, mono-oxolation) [19], the neutral precursor should be [WO $(OH)_4(OH_2)]^0$. One water molecule is bonded along the z-axis opposite to the W=O bond while the four OH groups are in the equatorial *xy* plane (Fig. 7-2-2b, c). In order to decrease electrostatic repulsions between highly charged cations, W^{6+} shifts toward the terminal oxygen (W=O bond) leading to strongly distorted WO_6 octahedra. Oxolation along equivalent *x* and *y* directions leads to the formation of the layered amorphous $WO_3 \bullet nH_2O$ gels or crystalline $WO_3 \bullet 2H_2O$ and $WO_3 \bullet H_2O$ phases. The $WO_3 \bullet 2H_2O$ and $WO_3 \bullet H_2O$ can be obtained via the acidification of a tungstate solution Na_2WO_4 through a proton exchange resin. $WO_3 \bullet H_2O$ can be obtain with a 100 ^{0}C heated environment during synthesis, and its structure is like in Fig.7-2-1c.

In the case of hydrothermal synthesis [20], the dielectric constant of water decreases as the temperature increases. Electrostatic repulsions between highly charged W^{6+} ions become stronger leading to the formation of more open structures such as hexagonal $WO_3 \bullet 1/3H_2O$ (Fig.7-2-3a). In the structures of hexagonal $WO_3 \bullet 1/3H_2O$ there is a corner which was occupied by a water molecule. These octahedra shared by four oxygens and form hexagonal assemblies in the *xy* plane. The layers stack along the *z* axis and are alternatively shifted by a/2 (Fig.7-2-3b). Fig. 7-2-3a shows a structural model based on

hexagonal WO_3, in which three- and six-membered rings of octahedra are displayed in the projected X-Y plane and four-membered rings are parallel to the vertical Z direction.

The three-member rings (Fig.7-2-3) can be ascribed to the W_3O_9 molecules produced during evaporation and sputtering [6, 21], and such molecules can be tied together to form six-member rings. Amorphous peroxotungstic acids have this kind of structure which is made of hydrogen bonded polyanionic species close to the paratungstate polyanion $[W_{12}O_{42}H_2]^{10-}$ [12] and so do the $WO_3 \cdot 1/3H_2O$ [14]. Our Raman spectra gave evidence for vibrations of W_3O_9 and terminal W=O bonds on internal surfaces (Table 7-6-1 and Section 7.6.6). This shows that there are octahedra and terminal W=O in the films.
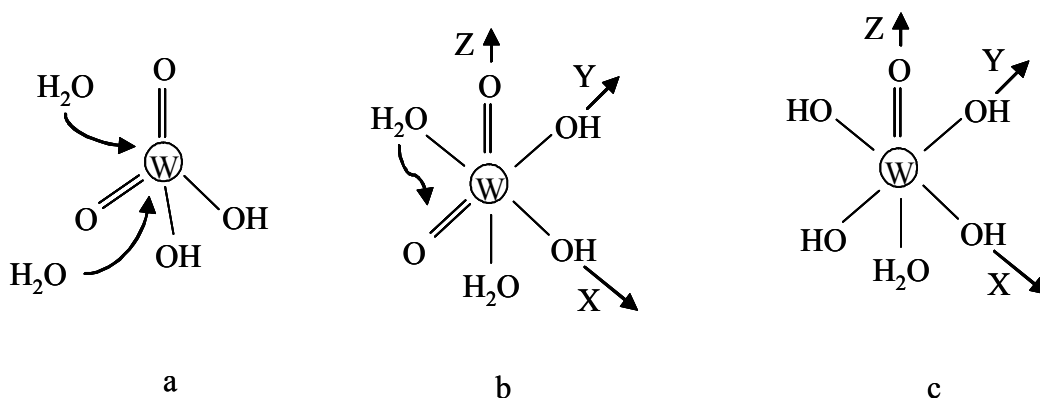

Fig. 7-2-2. Formation of $WO_3 \cdot nH_2O$ from the neutral precursor $[H_2WO_4]^0$

Generally the prepared α-WO_3 film containing a certain amount of water is of three kinds. H_2O molecules can attach into the film lattice during growth. They can be adsorbed on the film surface if the film is exposed to the atmosphere. WO_3 films can also be hydroxylated if they are exposed to a relatively humid environment.

Though the bulk crystals of the EC oxides are built from highly regular arrangements of edge-sharing or corner-sharing MeO_6 octahedra, the thin films rarely exhibit long-range order. In fact tetragonal, orthorhombic, monoclinic, triclinic, cluster, column and W_yO_x species are found in films due to atomic displacements, rotations of WO_6 – octahedra and deposition conditions [6]. During film growth, a cluster structure can be formed and arranged in space due to their hexagonal plate configuration. It is suggested that cluster growth and cluster-cluster linking is the typical case. The linking may be hydrogen bonds or water bridges. In addition, all of the EC oxides could be thought of as built up from MeO_6 octahedra in various corner-sharing and edge-sharing arrangements. The octahedra units are favorable both for ion and electron transport mechanisms.
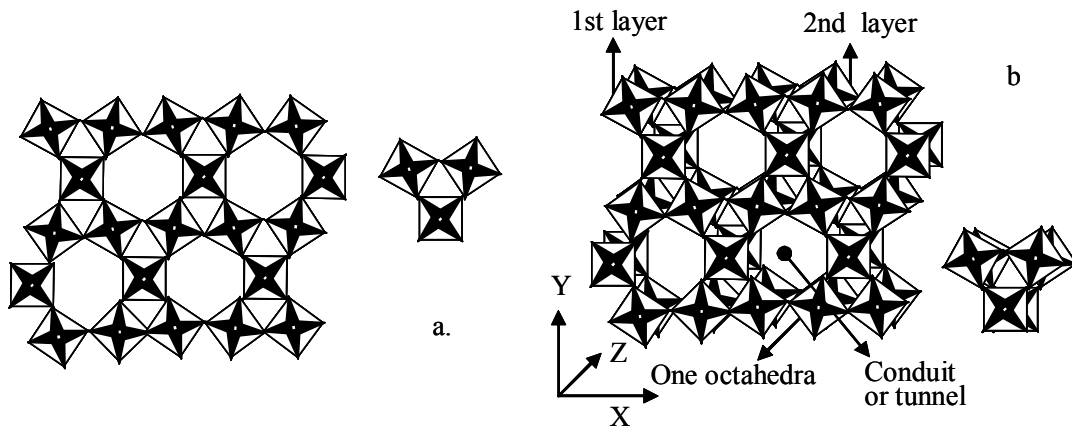
Fig. 7-2-3. (a) The six membered rings of (WO$_6$) octahedra sharing their corners in the *xy* plane or one layer hexagonal WO$_3$; (b) The hexagonal WO$_3$ structure showing the tunnels along the *z* axis; the relevant right structures are three membered ring cases.

7.3. WO$_3$ Films Grown with Different P$_{O2}$, Bias Voltages and Substrate Temperatures

7.3.1. Transmittance spectra

The films were deposited with different oxygen partial pressure ratios (P$_{O2}$), bias voltages and substrate temperatures (T$_s$). The transmittance spectra of the WO$_3$ samples were measured. The transmittance data of the samples deposited with −70 V bias, 1.3 Pa P$_T$ and in different P$_{O2}$ is listed in Table 7-3-1. Fig. 7-3-1a shows typical spectral transmittances of WO$_3$ samples deposited at 300 ^{0}C with -70 V bias voltage and different P$_{O2}$. In Fig. 7-3-1a, though the average intensity of the WO$_3$ curve is similar, the film deposited at higher P$_{O2}$ has a little better transmittance. It is found that the onset of the spectrum of the film deposited with 70% P$_{O2}$ is located at lowest position of the wavelength. This means there is a wider spectrum range in the case. Fig. 7-3-1b shows transmittance spectra of the WO$_3$ films deposited at different bias and different P$_{O2}$. The films deposited at both RT and 300 ^{0}C with different P$_{O2}$, presented the maximum transmittance (T$_{max}$) from 95% to 98%. The high value in the visible range is due to the wide optical band gap of WO$_3$.

In Fig. 7-3-1b, the effect of the bias was not significant on the transmittance of the films. It is found that the onset of the spectrum of the film deposited at higher

114

temperature is located at ~382 nm. It shifts towards longer wavelengths by ~23 nm comparing with films deposited at RT. This is related to the formation of bigger grains in the films due to the substrate heating, and a lower P_{O2} in the chamber.

For P_{O2} lower than 30%, the transmission clearly decreased due to the formation of metallic tungsten on the films. For P_{O2} higher than 80%, sputtering was not possible due to excess of oxygen on the sputtering atmosphere which results in target oxidation.

Table 7-3-1. Deposition conditions and parameters of WO_3 films deposited with -70 V bias voltage.

Sample	P_{O2}(%)	T_d(Min.)	d(nm)	δ(nm)	$T_{max.}$ (%)	E_g(eV)
			(	RT / 300^0C heated substrate		)
W1	80	50	471/364	4.7/4.5	98/98	3.48/3.45
W2	70	50	456/449	4.4/4.3	97/97	3.57/3.51
W3	60	42	516/571	4.2/4.1	97/98	3.46/3.36
W4	50	30	-	4.1/ -	96/97	3.43/3.35
W5	40	23	-	3.9/ -	95/96	3.48/3.35
W6	30	14	-	3.5/ -	95/97	3.53/3.39

Note. T_d:deposition time; d: thickness of film; δ: surface roughness; P_T: 1.3 Pa.
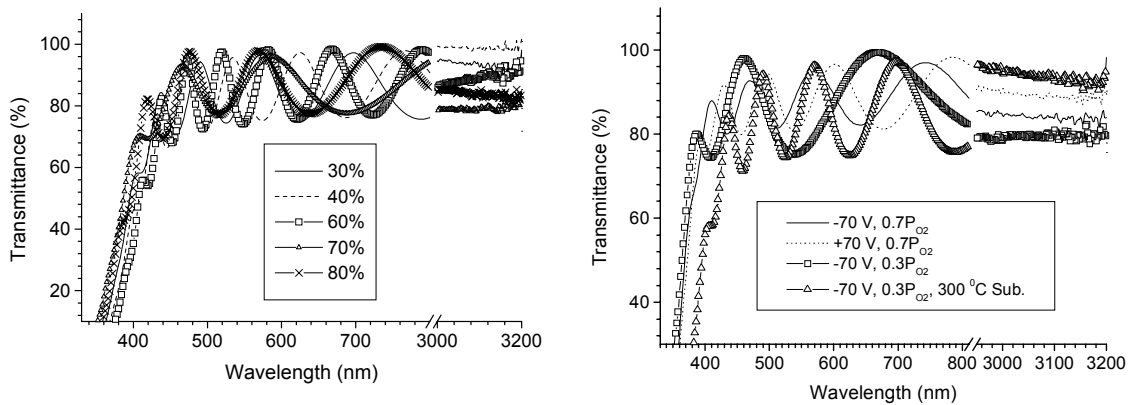

Fig.7-3-1. (a) Transmittance spectra of WO_3 films deposited at 300 ^{0}C and with different P_{O2} (oxygen partial pressure). (b) Transmittance spectra of WO_3 films deposited at different bias voltage and different P_{O2}.
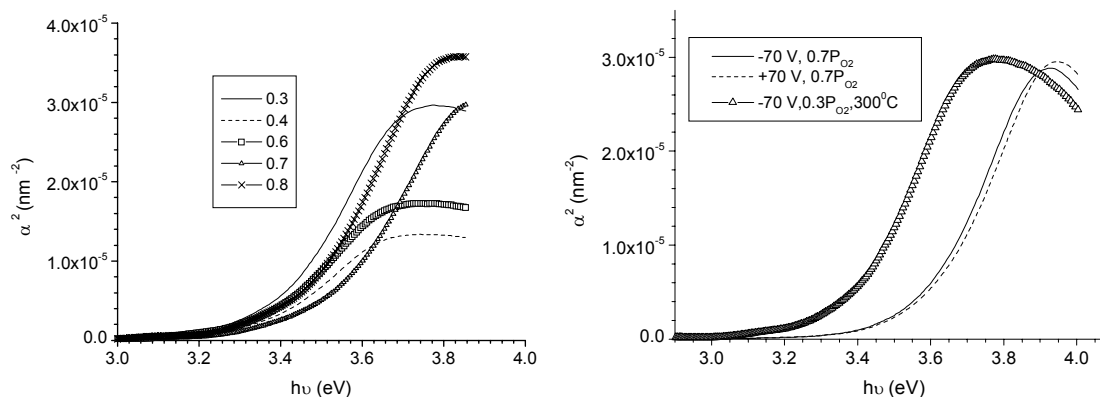
Fig. 7-3-2. Dependence of the absorption coefficient on the photo-energy. (a) WO_3 films prepared at 300 ^{0}C and with different P_{O2}. (b) WO_3 films prepared with different bias and different P_{O2}.

7.3.2. Absorption and optical energy band gap E_g

The absorption coefficient α in the case of a direct transition semiconductor (Section 3.7) can be determined as $\alpha^2 = C$ (hv - E_g). Extrapolating the linear region towards the hv axis gives the effective direct transition energy E_g. These values are in Fig. 7-3-2 (a, b) and listed in Table 7-3-1. The obtained E_g values are in the range 3.35 - 3.57 eV for WO_3 films deposited at RT and 300 ^{0}C with different P_{O2}. It is observed that the optical band gap reaches a maximum of 3.57 eV for the sample with 70% P_{O2} and has smaller values for 40% – 60% P_{O2}. The effect of the positive or negative bias is not clearly significant in the E_g of the films (in Fig. 7-3-2b).

7.3.3. AFM study of the surface micro-structure of the films deposited with different bias

In order to optimize the properties of the WO_3 films, a bias potential (U_{bias}) was applied in the substrate during deposition. Fig. 7-3-3 shows the topography of three films prepared by d.c. sputtering at RT with 70% P_{O2} and with different applied bias voltages (+60, 0 and -60 V). If U_{bias} is positive, then electrons and negative ions bombard the surface. If U_{bias} is negative the surface is bombarded by positive ions. The photographs show different surface topography for positive and negative U_{bias}.

Fig. 7-3-3a shows that for electron bombardment the surface is very rough with bumps originated from the columnar growth (Section 7.4.2 and Section 9.4) of the

116

films. The bump height is ~20 nm and their average separation is less than 0.1 μm. The electron bombardment of the surface gives energy to already deposited atoms so that they can diffuse to occupy crystal positions. Thus, these films are more crystalline as observed in the X-ray spectra [4]. These spectra show that the films present a WO_3 phase with an increased crystallinity (smaller peak width) as compared to the corresponding films deposited without bias voltage.
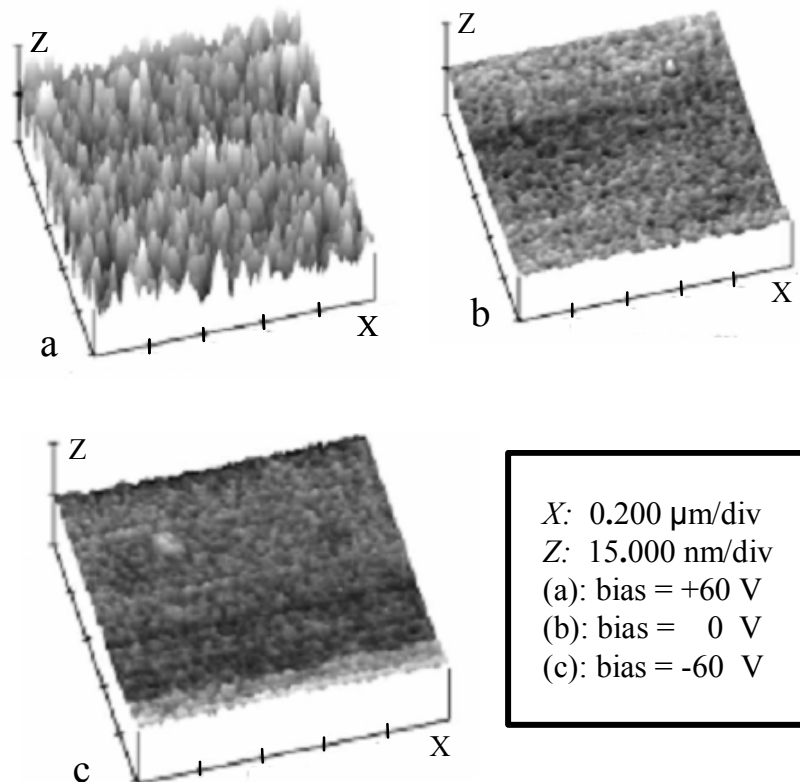

X: 0.200 μm/div
Z: 15.000 nm/div
(a): bias = +60 V
(b): bias = 0 V
(c): bias = -60 V

Fig. 7-3-3. AFM of the surface of the tungsten oxide films deposited at room temperature with 70% P_{O2} and with an applied bias voltage: (a)U_{bias} = +60 V; (b)U_{bias} = 0 V; and (c)U_{bias} = -60 V.

On the other hand, positive ion bombardment (negative bias) disrupts the columnar structure and promotes denser and smooth films [23, 24]. This induces the formation of a smooth surface as observed in Fig. 7-3-3 (c) for the film deposited with U_{bias} = -60 V. The X-ray spectra of the films show that this bombardment induces an increased amorphisation of the tungsten oxide as compared to the corresponding films deposited without bias voltage. The effect of electron and ion bombardment is not so sharp on the optical properties of the films. Their transmission spectra are similar (Fig. 7-3-1b).
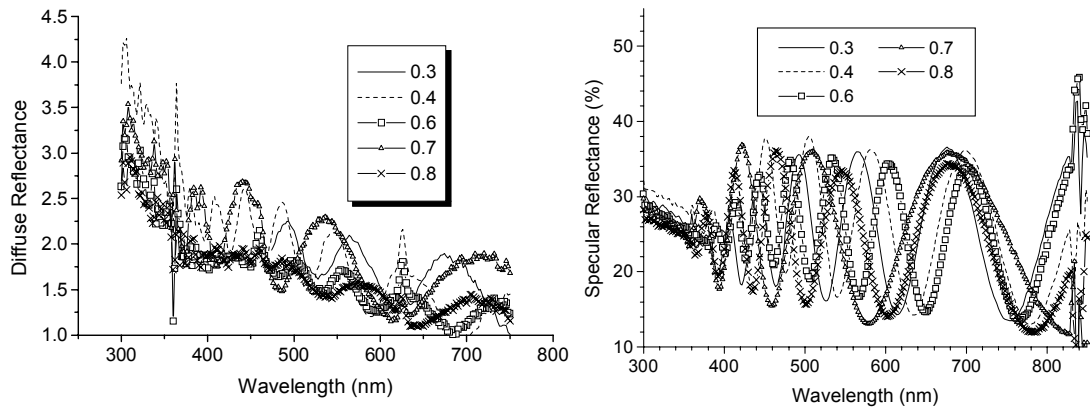
Fig. 7-3-4. Diffuse reflectance (DR) and specular reflectance (SR) of the WO$_3$ films deposited at 300 ^{0}C and with different oxygen partial pressures.
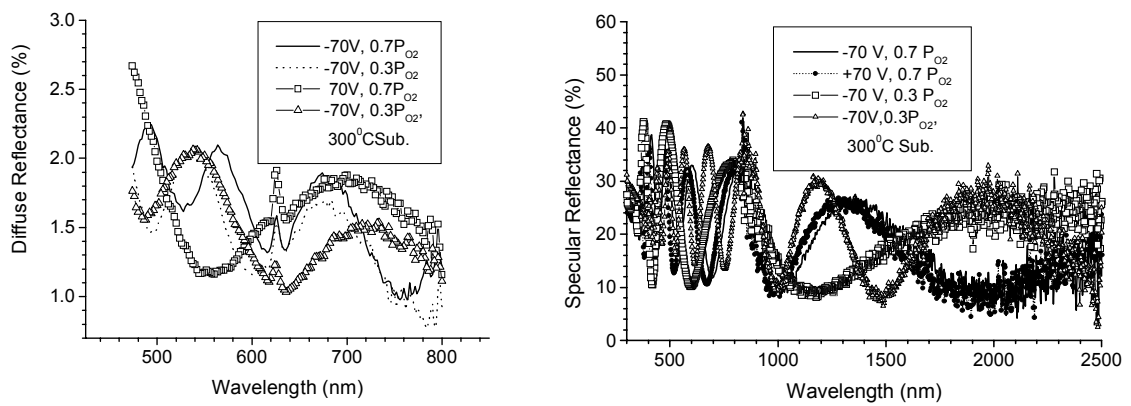

Fig. 7-3-5. The diffuse reflectance (DR) and specular reflectance (SR) of the WO$_3$ films deposited with different bias and oxygen partial pressures.
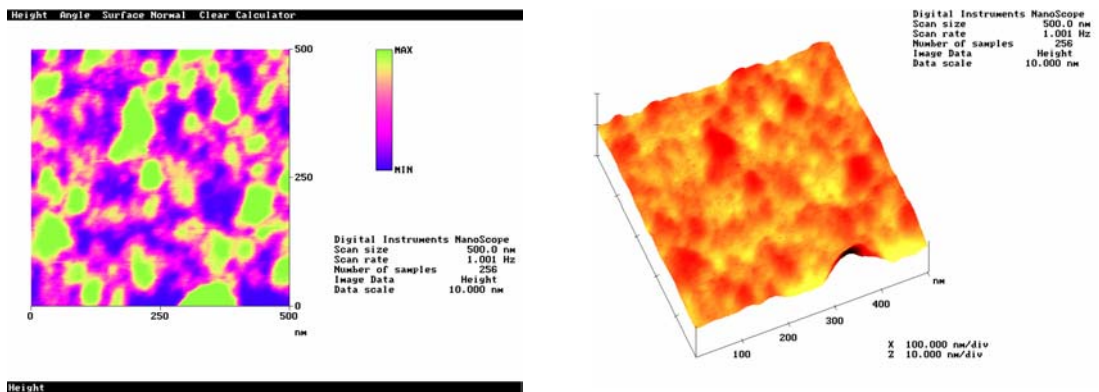

Fig. 7-3-6. AFM topography of the WO$_3$ film deposited with 70% oxygen partial pressure, -70 voltage bias and room temperature.

118

7.3.4 Surface roughness of the films

Surface roughness (δ) is an important parameter of thin films [25]. To calculate δ of the WO$_3$ films, diffuse reflectance (DR) and specular reflectance (SR) were measured (Fig. 7-3-4 and 7-3-5). The DR spectra of the WO$_3$ films exhibit similar shapes and very low intensity (less than 4.8%). Qualitatively this presents micro size composition and its average distribution of the film. The SR spectra of the WO$_3$ films also exhibit similar shape and about 25% average intensity. The films present micro size grain boundaries and smooth surface. The δ values range from 3.5 nm to 4.7 nm in the analyzed samples, and were calculated by TIS (total integrated scattering, Section 3.3 of Chapter 3). The AFM observations supported these results. Because our WO$_3$ are good transparent thin films, we conclude that the reflectance mainly comes from interface of the film. Fig. 7-3-6 shows a typical AFM micrograph of the surface of the film. The surface roughness and nanometer grain boundaries are shown in the figure. The average grain size (top view of the sample surface) is 30 nm, the average height of δ is less than 5 nm.

7.3.5. Conclusion of the section

The optimization of the WO$_3$ films with different structures were achieved by applying a bias potential (U$_{bias}$) during deposition. The films deposited at both RT and 300 ^{0}C substrate temperatures with different P$_{O2}$, presented the maximum transmittance (T$_{max}$) ranging from 95% to 98%. Though the average intensity of the WO$_3$ curve is similar, the films deposited with higher P$_{O2}$ have better transmittance. The 70% P$_{O2}$ WO$_3$ film has a wider spectrum range. Bigger grains were formed in the films deposited at high temperature and lower P$_{O2}$. The optical measurements show a change in transmission and optical band gap with different P$_{O2}$. This indicates that the optical properties are dependent on the oxygen deficiency in the films. It was observed that the E$_g$ values of the films are in the range 3.35 - 3.57 eV. The discussion of AFM and XRD results show that the electron bombardment favors the formation of more crystalline films and ion bombardment favors the amorphisation of the tungsten oxide phases in the films. The effect of positive or negative bias has no clear effect in the optical properties of the films. From AFM results the average grain size of the films is ~30 nm, and from TIS calculation the average height of δ is less than 5 nm.

7.4. Micro-structure and Annealing Effect of WO$_3$ Films and Mo Doped WO$_3$ Films

7.4.1. Transmittance spectra

The depositing condition of the WO$_3$ films was chosen with 70% P$_{O2}$, 1.3 Pa P$_T$ and -70 V bias and they are shown in Table 7-4-1. The transmittance spectra of WO$_3$ samples annealed in air and heated at 300 ^{0}C are shown in Fig. 7-4-1a. It is seen that there are some differences between the films annealed below 300 ^{0}C and at 300 ^{0}C heated substrate. It is found that the onset of the spectrum of the film deposited at RT, annealed at 160 ^{0}C and 300 ^{0}C is located at ~363 nm. The onset of the spectrum of the film deposited at 300 ^{0}C shifts towards longer wavelengths (380 nm or red shift by ~17 nm). This is related to the formation of bigger domains in the film (Section 4). There are not clear differences between the transmittance of Mo doped WO$_3$ films (Fig. 7-4-1b) and pure WO$_3$ films, however the film with more than 6% Mo dopant has a red shift in transmittance. It was also confirmed by SEM that the 6% Mo doped WO$_3$ film has bigger grains (Section 7.4.2).

Table 7-4-1. Deposition conditions and the parameters of Mo doped WO$_3$ films deposited with −70 V bias voltage.

Sample	P$_{O2}$(%)	d(nm)	T$_s$(^{0}C)	T$_{max.}$ (%)	Ratio of Mo(%)
WM1	70	465	RT	98	6.0
WM2	70	465	RT	98	5.0
WM3	70	456	RT	97	3.8
WM4	70	456	RT	97	1.9
WM5	60	522	RT	98	5.0
WM6	60	518	RT	97	3.8
WM7	70	442	300	98	3.8
WM8	70	438	500	98	3.8

7.4.2. Micro-topography of the films

Similarly to Section 7.3.4, the DR and SR spectra of the WO$_3$ films were measured. The DR spectra exhibit similar shape and very low intensity (less than 3.4%). The SR spectra exhibit reflectance less than 30.2%. From the calculation and AFM analysis the roughness δ values of the samples are less than 5 nm. The random bigger grain size appears in the film samples (Fig.7-4-2).
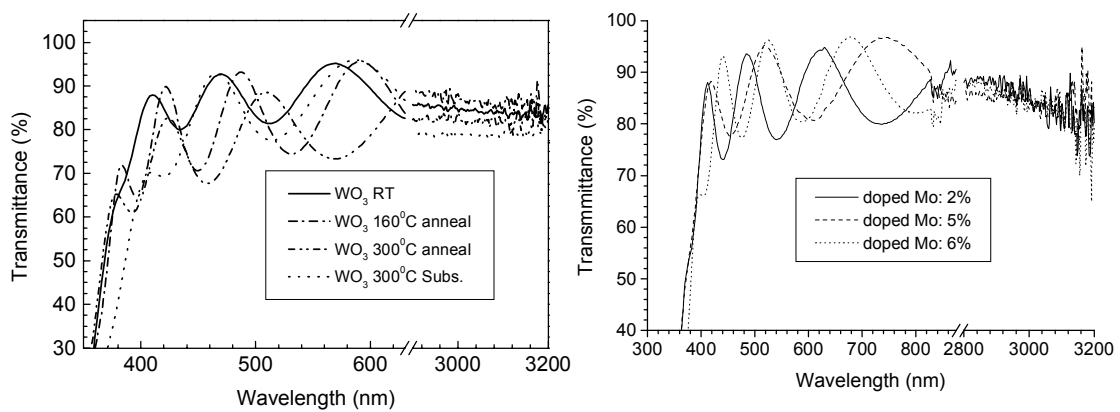
Fig. 7-4-1. Transmittance spectra of WO$_3$ films which deposited with -70 V bias and 70% P$_{O2}$. (a) At room temperature (RT), annealed at 160 ^{0}C, annealed at 300 ^{0}C and 300 ^{0}C heated substrate; (b) With different ratios of Mo dopants.
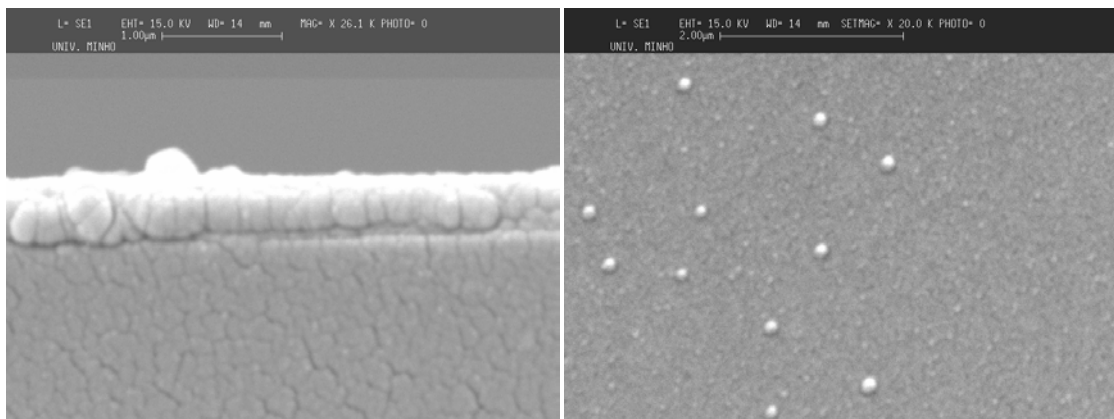

Fig. 7-4-2. SEM cross section and micro-topography of the 6% Mo doped WO$_3$ film (WM1) prepared by sputtering at RT with 70% P$_{O2}$ and -70 V applied bias voltage.

Fig.7-4-2 shows the SEM micro-topography and cross section of the 6% Mo doped WO$_3$ film (WM1) prepared by sputtering at RT with 70% P$_{O2}$ and -70 V applied bias voltage. The as deposited film has a smooth surface and a columnar growth structure. Generally a physical model can be chosen for simulation of columnar growth in PVD (physical vapor deposition) deposition. From the model based on ballistic aggregation of structural units and ensuing re-accommodation of these balls, as well as from growth instabilities in continuum theories [26], the formation of columnar structures can be understood. Columns with linear sizes exceeding 100 nm are included in structural zone diagrams (Zone 2 in the Thornton diagram). For films prepared by normal evaporation

the vapor flux has perpendicular incidence towards the substrate. The columns are then oriented normal to the substrate. It is possible to increase the columnar character by depositing WO_3 films at an oblique angle. If the vapor flux had an angle 72^0 from the substrate normal, the column inclination angle is $\sim45^{0}$ [27].

Some big particles distributed randomly on the surface of the films were found in both Fig. 7-4-2. By EDX analysis, these particles consist of formation of MoO_3 doped WO_3. Through the film formation theory[69, 70], big particles and domain distributed randomly can be explained. Nordlund and Averback [28] indicated that the diffusion coefficient of atoms with high melting point is smaller than that of atoms with low melting point, during the relaxation period from studies by ion-beam mixing techniques. Furthermore, from the sputtering results, the diffusion coefficient of W atoms is smaller than that of the Mo atoms in the process. Since the Mo atomic weight (95.94) is much smaller than that of W (183.85) [29] and the mobility of the Mo atom is higher than that of the W atom, the relaxation process is mainly limited by the relaxation behavior of the W atoms in the atomic collision period. The higher mobility of the Mo atoms can cause formation of bigger particles in some places of the film, but does not form aggregates of Mo atoms themselves.
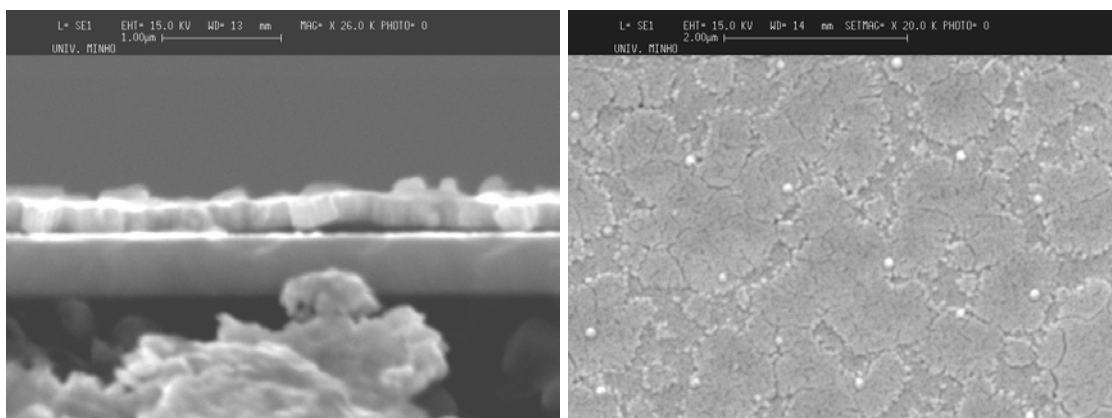

Fig. 7-4-3. SEM cross section and micro-topography of the 6% Mo doped WO_3 film after 400 ^{0}C annealing in air (The film prepared at RT, 70% P_{O2} and -70 V applied bias voltage).

The SEM micrograph of the same sample-WM1, but annealed at 400 ^{0}C in air, is presented in Fig.7-4-3. After annealing, the bigger domains are formed, the cracks and spalls appear in the film.

7.4.3. X-ray diffraction of WO₃ and Mo doped WO₃ films

The W-O system is rather complex with a large number of phases [12, 13] and quite different from a simple cubic structure [30], as mentioned in 7.2.1. In this section XRD was used to analyze the structure. In the experiments, amorphous WO$_3$ films were obtained at RT and annealed at temperature below 300 ^{0}C. Fig. 7-4-4a shows the XRD diagrams of the WO$_3$ as deposited (1), annealed at 160 ^{0}C (2), 220 ^{0}C (3), 300 ^{0}C (4) and 500 ^{0}C (5).
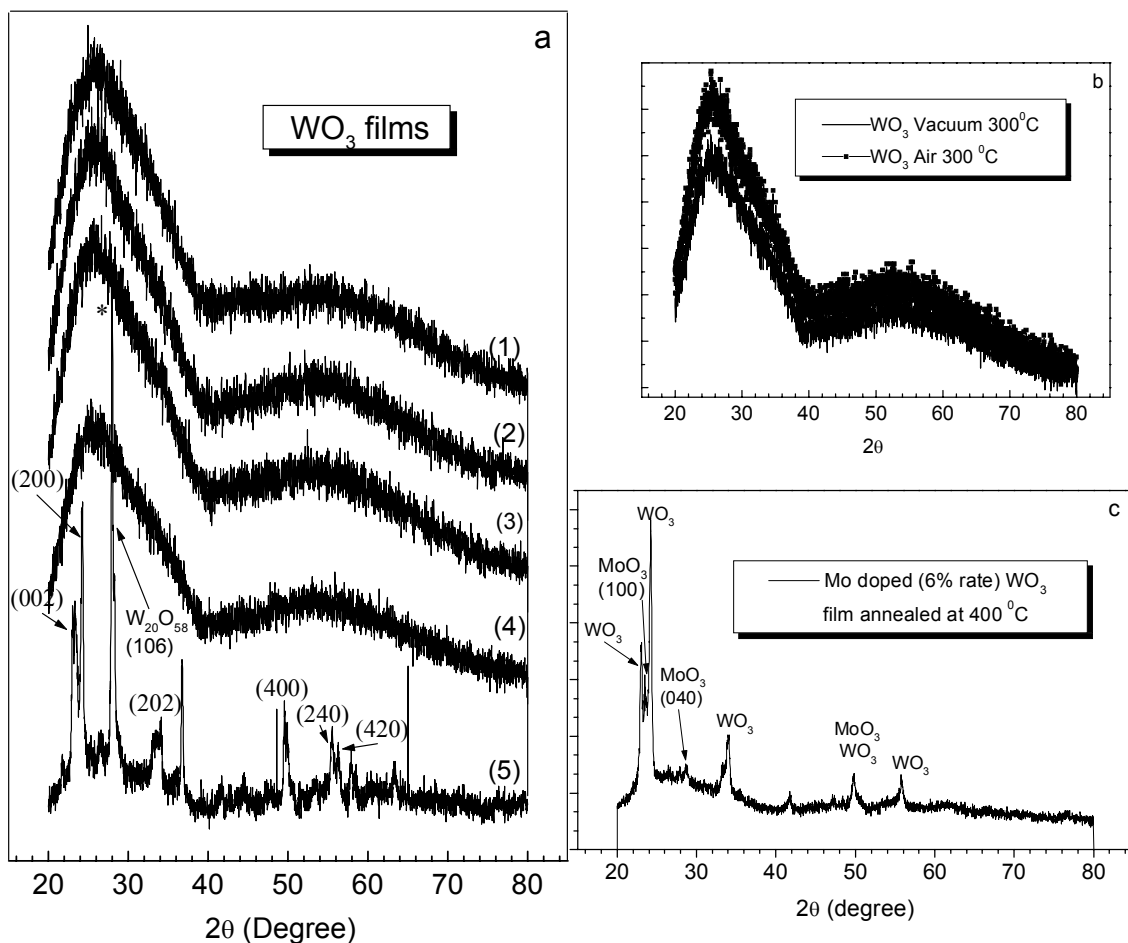

Fig. 7-4-4. (a) X-ray diffraction (XRD) diagrams of WO$_3$ as deposited (1), annealed at 160 ^{0}C (2), 220 ^{0}C (3), 300 ^{0}C (4) and 500 ^{0}C (5). (b) The XRD diagrams of WO$_3$ annealed at 300 ^{0}C in vacuum and air. (C) 6% Mo doped WO$_3$ film annealed at 400 ^{0}C in air.

It was found that films deposited with 70% P$_{O2}$, at RT, low T$_a$ and low T$_s$ (less than 300 ^{0}C), present similar XRD of amorphous WO$_3$ [weak peaks at 25.96 (0 0 1) and 53.80 (0 0 2)]. It was found that films deposited with low P$_{O2}$ (less than 0.5) and low temperature (less than 300 ^{0}C), are also amorphous. When P$_{O2}$ increases the structure of the film starts to change. For P$_{O2}$>0.5 the films present a mixture of WO$_3$ phases that

123

include $W_{20}O_{58}$ ($2\theta=27.99$). To determine the oxygen concentration where the $W_{20}O_{58}$ starts to appear, the relative X-ray intensity of the peaks for each sample as a function of P_{O2} was studied. It was observed that the structural change began at $P_{O2}=0.6$ in room temperature. This effect is enhanced for higher deposition temperatures. For high P_{O2} the WO_3 phase is more ordered and the $W_{20}O_{58}$ oxygen deficient phase is increased. Because of amorphism of the sample, XRD could not give more information of structures for such a thin α-WO_3 film. Since Raman spectroscopy is more sensitive to the local environment of the molecular arrangements, we will discuss Raman analysis on α-WO_3 films in Section 7.6.

Fig. 7-4-4b shows the XRD diagrams of WO_3 annealed at 300 ^{0}C in vacuum and air. They are similar to the as-deposited film at RT. The as-deposited WO_3 films have no sharp peak in their X-ray diffraction spectra. From the XRD data and curve fitting analysis a broad peak at 26.0 (001) and 28.0 (106), a mixing broad peak consisting of 53.80 (002), 55.60 (240) and 56.20 (420) peaks plus broad background from the glass substrate were observed. Clearly the films are amorphous and very thin. After annealing in air at 500 ^{0}C for 1 hour, the sharp and strong peaks of (002), (200), (202), (400), (240) and (420) planes of a monoclinic phase appear in curve (5) of Fig. 7-4-4a. Fig. 7-4-4c shows the XRD diagrams of 6% Mo doped WO_3 annealed at 400 ^{0}C in air. Sharp and strong WO_3 and MoO_3 peaks appear in the XRD pattern.

Similar to the annealing case, the WO_3 film which was deposited at more than 400 ^{0}C substrate temperature has strong (002), (200), (202), (400), (240) and (420) peaks. This can be explained as follows. When the film is deposited at RT, the collision relaxation period may not be long enough for the system to arrive to the ordered phase state, as the W atoms do not gain enough kinetic energy from the atomic collisions. Thus the system is in the amorphous state. When the substrate temperature is increased to 400 ^{0}C, the relaxation period is longer and the W atoms are more active so that the system begins to undergo a structural rearrangement.

7.4.4.   XPS of the WO_3 films

Here XPS is used to confirm that the film is composed by WO_3. Fig.7-4-5 shows the evolution of the W 4f doublet peak of WO_3 deposited with -70 V bias and 70% P_{O2} before and after 400 ^{0}C treatment. They have the same characteristics as bulk WO_3. It consists of a single doublet at binding energies 35.6 eV for the W $4f_{7/2}$ and 37.5 eV for the W $4f_{5/2}$. W $4f_{7/2}$ corresponds to tungsten in the +6 oxidation state (W^{6+}) of WO_3.

After annealing at 400 ^{0}C in air all peaks had a slight shift in the direction of low energy.
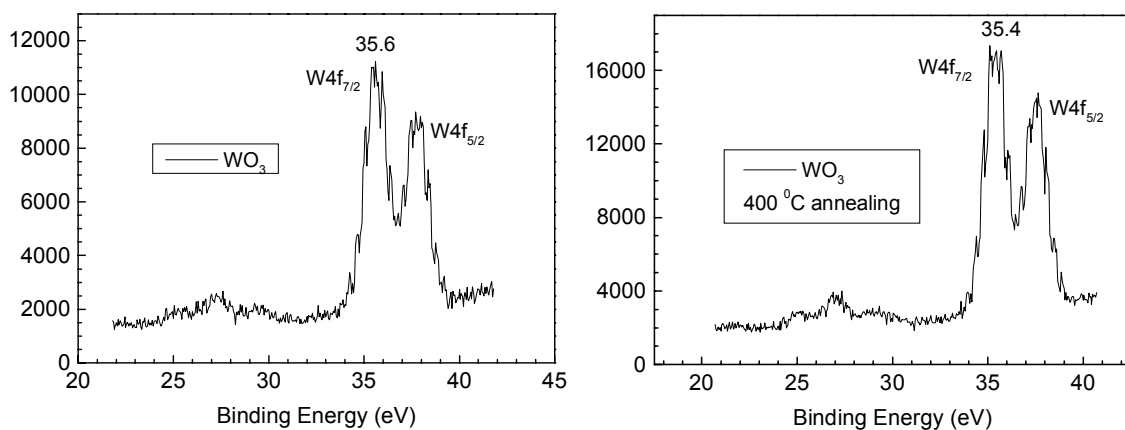

Fig. 7-4-5. X-ray photoelectron spectra of W 4f doublet of WO_3 (sample-W2) deposited at −70 V bias in 70% P_{O2} before and after annealing at 400 ^{0}C.
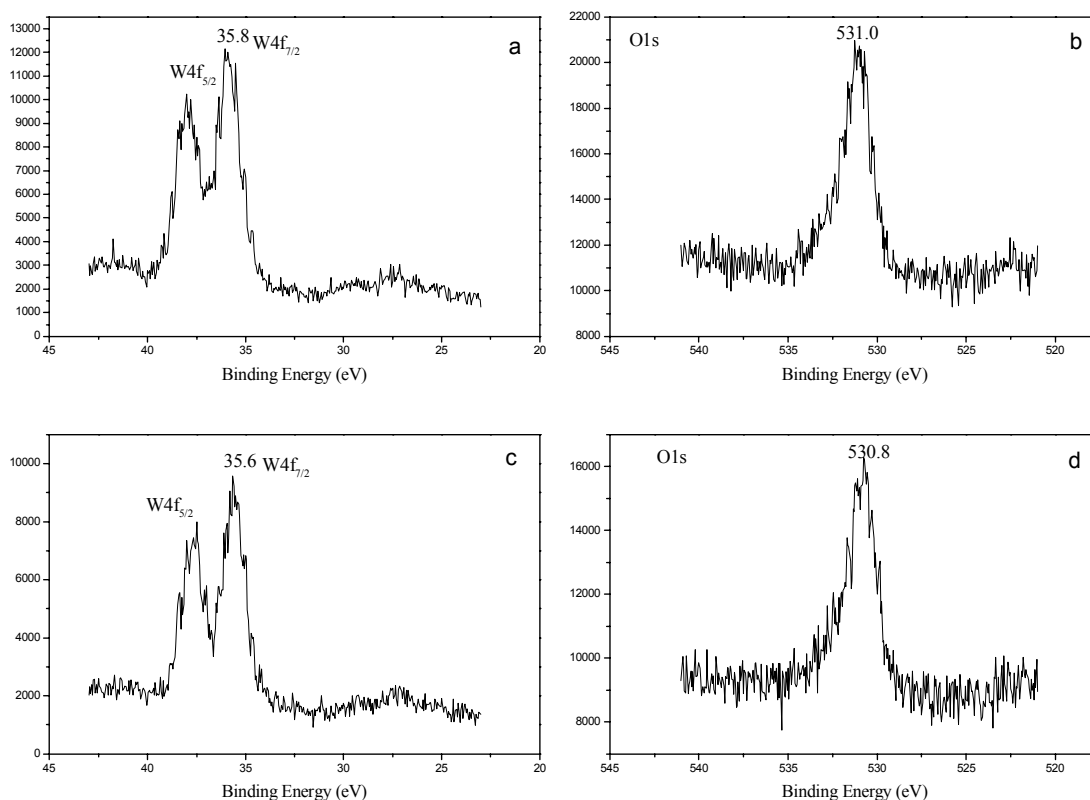

Fig. 7-4-6. X-ray photoelectron spectra of the W 4f doublet and the O1s peaks of WO_3, (a, b) as deposited with +70 V bias and 70% P_{O2}; (c, d) as deposited with -70 V bias and 30% P_{O2}.

The shape of the W 4f peak changes with increasing temperature. From the XPS spectrum of the annealed films the W $4f_{5/2}$ /W $4f_{7/2}$ ratio of the two peaks becomes

stronger after annealing. This means that the oxidation state is lower than +6. In addition the prepared α-WO$_3$ films contain a certain amount of water as described in Section 7.2.4. All this indicates that during the 400 ^{0}C heat treatment, oxygen or adsorbed water molecules leave from the film. This phenomenon can also be due to the surface roughness and the appearance of oxygen cavities in the films. The XPS of the WO$_3$ films, which were deposited at RT, different bias and different P$_{O2}$, were measured too as a comparison. Fig. 7-4-6 (a, b) shows the W 4f doublet and the O1s peaks of WO$_3$ deposited with +70 V bias and 70% P$_{O2}$. The peaks have a slight shift to direction of high energy. Fig. 7-4-6 (c, d) shows the W 4f doublet and O1s peaks of WO$_3$ deposited with -70 V bias and 30% P$_{O2}$. The XPS O 1s peak at a binding energy of 530.8 eV assigned to the oxygen in WO$_x$ [31].

7.4.5. Conclusions of the Section

There are differences in transmittance between the films annealed below 300 ^{0}C and deposited at 300 ^{0}C. The spectrum onset of the WO$_3$ as-deposited film at 300 ^{0}C shifts towards longer wavelengths by ~17 nm (380 nm) comparing to all others. From the calculations and AFM analysis the roughness δ values of the samples are less than 5 nm in an area of 500 x 500 nm. One random bigger grain (~110 nm) appears or does not appear in any one square μm area on the films. The less than 6% Mo doped WO$_3$ film, prepared by sputtering at RT in 70% P$_{O2}$ with -70 V applied bias voltage, presented a smooth surface and had columnar growth structures like pure WO$_3$ films. The SEM observation supported all the above results. XRD and XPS was used to analyze the sample structure and confirmed that the film is WO$_3$ or MoO$_3$ doped WO$_3$ films. It was observed from XRD that the films present an amorphous WO$_3$ phase at RT and less than 300 ^{0}C annealing. The as prepared WO$_3$ films have no sharp peaks in their X-ray diffraction spectra. From the XRD data of deposited WO$_3$ films and curve fitting analysis a broad peak at 25.96 (0 0 1) and 27.99 (10 6), a mixing broad peak consisting of 53.80 (002), 55.60 (240) and 56.20 (420) peaks plus broad background from the glass substrate were observed. After annealing in air at 500 ^{0}C for 1 hour, sharp and strong peaks appear corresponding to the peaks (002), (200), (202), (400), (240) and (420) of a monoclinic phase. XRD diagrams of WO$_3$ annealed at 300 ^{0}C in vacuum and air are similar to the films deposited at RT without annealing. The results show that for low P$_{O2}$ they present an amorphous WO$_3$ phase, while for high P$_{O2}$ they present a mixture of a more crystalline WO$_3$ phase and a W$_{20}$O$_{58}$ oxygen deficient phase. The W 4f and O1s

peaks of as deposited WO_3 with different bias and P_{O2}, before and after 400 ^{0}C treatments, were observed. They consist of a single doublet at binding energies 35.6 eV for the W $4f_{7/2}$ and 37.5 eV for the W $4f_{5/2}$. W $4f_{7/2}$ corresponds to tungsten in the +6 oxidation state (W^{6+}) of WO_3. The rate W $4f_{5/2}$ /W $4f_{7/2}$ of two peaks become stronger after annealing. The results indicated that during a 400^0C heat treatment oxygen or adsorbed water molecules can leave from the film.

7.5. Study of Tungsten Oxide Thin Films from the Mid Infrared to the Ultraviolet Spectral Region

7.5.1. Introduction

The study of UV-Vis-NIR on α-WO_3 films has been exploited in the development of smart windows [5], but the far infrared region has also significance for EC materials and its devices. Mid-IR reflectance modulation in WO_3 is possible at thermal wavelengths (8-12 μm) creating possibilities for the development of smart infrared devices with application on temperature control of satellites where radiant heat transfer is the prime mechanism [32]. M. G. Hutchins et al [33] and A. Rougier [34] had further investigated the mid-infrared spectra, IR optical properties and their constants. In addition the structure and component of the material control the property of the thin film. Mid-IR spectrum is also a powerful tool to analyze and investigate the structure and components of a material. Gabrusenoks et al have given some brief statement about vibrations in the range 100-400 cm^{-1} [35]. Here we use mid infrared absorption spectra to characterize the structure of WO_3 films. Most infrared (IR) commercial systems have a frequency range of 400-4000 cm^{-1}. In practical applications the WO_3 films should be deposited on normal glass for smart windows. Since the glass has a limited transmittance range of 2000-4000 cm^{-1} in the infrared, we used mid-infrared reflective absorption spectra to study WO_3 films in both 400-2000 and 2000-4000 cm^{-1} ranges. With this technique, it is possible not only to identify different oxide phases but also to detect intercalated or absorbed H_2O.

7.5.2. IR vibrations of tungsten oxides

WO_3 consists of packed corner-sharing WO_6 octahedra, contains 4 atoms and 6 fundamental normal modes of vibration. The observed vibration bands are mainly the fundamental vibrations of W═O, W-O and W-O-W chromophores. The local symmetry

of the W=O chromophore allows the separation of normal modes according to the direction of their dynamic dipoles, helping the assignment of IR active vibrations. For molecular structure and orientation determination, the most relevant normal modes are the stretching vibrations (ν), in-plane bending vibrations (δ) and out-of plane wagging (γ) modes.

Due to IR high sensitivity in the presence of the OH group, direct experimental proof of the presence of water in the films can be deduced from the IR spectrum. This is important due to the role-played by water in the EC mechanism. IR spectra of α-WO_3 films and polycrystalline WO_3 are similar. Their maximum in the frequency range of deformation vibration (100-400 cm^{-1}) does not differ. The center of gravity for the IR absorption bands in this region is the same [9, 34-35].

Table 7-5-1. Summary of the IR assignment of the WO_3 film samples

Group	Wavenumber (cm^{-1})			assignment	note
	Experimental		Ref.	(Structure number)	
	RT	$T_{s:}$ 300 ^{0}C			
W-OH…H_2O	3506	3506	3498 [41]	$\nu_{sym(OH)}$ - $\nu_{asym(OH)}$ [18]	#1
O-H	2923	2923	2200- [43]	ν_{OH}	
-	1985	1939	-	-	
OH, H-O-H	1613	1613	1610[41, 43]	(a) δ_{OH} in W-OH,	
				(b) $\delta_{(OH O)}$	
OH , W-O	1453	1455	1436[34, 37]	ν_{OH}, δ_{OH}	#2
			1400[41]	ν_{W-O}	
-	1327	1327	-	-	
W-OH	1142	1167	1156[36]	δ_{W-OH}	
W=O, W-O	990	982	995[41]	ν_{W-O}	
W-O-W	884	853	874[62]	W_3O_9	
W-O-W	670	670	670[41]	γ_{W-O-W}	
O-Lattice	500	515	500[36, 39]		#3
W-O	417	417	418[41]	δ_{W-O}	

Note: All H_2O means the adsorbed molecular water. #1: attributed to the OH stretching vibration of W-OH…H_2O groups. #2: attributed to the OH group bonded to either H_2O or surface oxygen atoms of the film. #3: assigned to the strong coupling of the oxide lattice.

The IR data of our samples, assignment of characteristic vibration wavenumber, and corresponding references are shown in Table 7-5-1. The IR spectra of WO_3 deposited at RT and −70 V bias in 70% P_{O2} are constituted with many broad peaks in the region 1453-3600 cm^{-1} (Fig. 7-5-1, curve1). A broad band in the 3250-3600 cm^{-1} region, and two peaks located at 1613 cm^{-1} and 1453 cm^{-1} are badly resolved. Those bands originate from moisture and are assigned to ν(OH) and δ(OH) modes of adsorbed water. Especially from the 1453 cm^{-1} peak it is deduced that an OH group is strongly bonded

to either water molecules or to surface oxygen atoms [34, 37]. We find evidence for the formation of OH groups in the spectral range between 1453 and 3600 cm^{-1}. In the region of >3700 cm^{-1} the samples exhibit a very high transmittance due to a low absorption character.

The main tungsten oxide vibrations are found in the infrared regions of 1453-400 cm^{-1} and 3506 cm^{-1}, which correspond to tungsten-oxygen stretching, bending and lattice modes. The spectra of hydrated amorphous films had been studied previously [38]. Here we find some relatively strong and weak bands at 417, 500, 670 (690) and 990 (970) cm^{-1} from Fig. 7-5-1. The 500 cm^{-1} band is assigned to the strong coupling of the oxide lattice in hydrated $WO_3 \bullet nH_2O$ material [36, 39]. The 670 cm^{-1} band is assigned to the out of plane deformation W-O-W mode, when hydrogen is located at a coplanar square of oxygen atoms. Sienko [40] and Wright [36] had contradictions about if there are the 670 and 500 cm^{-1} bands. We deduce that this is possibly due to the problem of the IR instruments at their time.
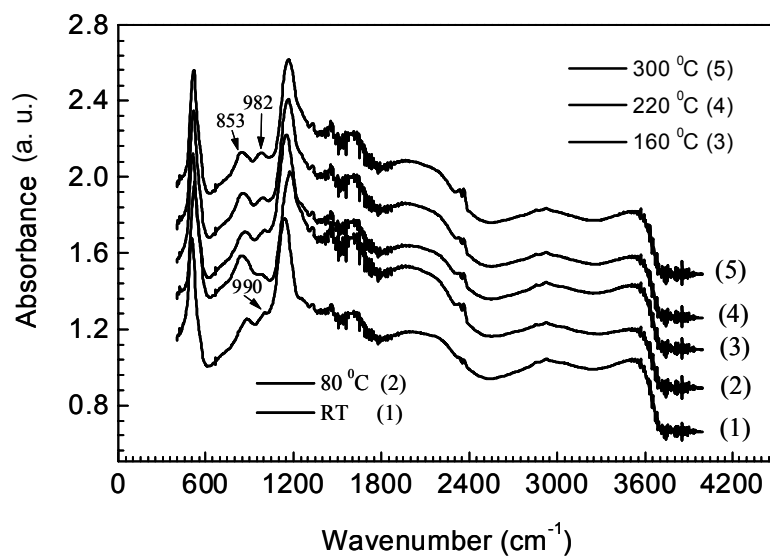

Fig. 7-5-1. Reflective absorption IR spectra of WO_3 (sample-W2) films deposited at room temperature (RT) and annealed at different temperatures.

A relatively strong band at 1142 cm^{-1}, which is assigned to the plane deformational (bending) W-OH mode, was found. It was also observed in the inelastic incoherent neutron scattering (IINS) spectra [36]. The strong peak at 1142 cm^{-1} is assigned to δ(OH) in W-OH group.

The ex-situ IR spectra of films, which were deposited at RT and –70 V bias in 70% P_{O2}, were measured after annealing the films at 80, 120, 220 and 300 ^{0}C for 1 hour. Their FTIR spectra are compared in Fig. 7-5-1. As it is known, the tungsten-oxygen modes have a red shift after annealing, because the creation of weakly bonded W-OH groups is formed in the as-deposited film. In the frequency range 400-1300 cm^{-1}, the shoulder around 982 cm^{-1} (W=O terminal modes of surface grains) and W-O-W bridging mode 853 cm^{-1} rises after at different temperature annealings. These behavior was also observed for the films deposited with –70 V bias in 30% P_{O2} and +70 V bias in 70% P_{O2}. A typical band 853 cm^{-1} of the weakly crystallized monoclinic (m) WO_3 (m-WO_3), which has much lower symmetry was formed, increased with increasing annealing temperature [41]. Raising the temperature to 80 ^{0}C produces a well-resolved 853 cm^{-1} band (Fig. 7-5-1). The transformation to the m-WO_3 phase can be seen from the change of the 982 cm^{-1} band. The removal of water causes a stronger W=O bond, as can be clearly seen by the inverse order of formation of $WO_3 \cdot nH_2O$ in Fig. 7-2-2. Distortions in the films are due to the presence of –OH groups, which affect the site symmetry (S_6) of the WO_6. The Raman experiments supported the existence of the 982 and 853 cm^{-1} band. The general broadness of the IR peaks confirmed the film amorphous nature as observed by X-ray diffraction. Since during the operation of the IR there is absorbed water on the surface of the films, there are some similar ties between the IR spectra of RT grown and annealed samples. In addition, the IR spectra of all samples exhibit similar shapes and low absorption intensity in the range 4000 cm^{-1} (2.50μm)-1800 cm^{-1} (5.56 μm).

7.5.3. Transmittance and reflectance of WO_3 films in the UV-Vis-NIR regions

Transmittance: Some transmittance spectra of the films are shown in Fig. 7-5-2. They were deposited with -70 V bias, 70% P_{O2}, and post-annealed at different temperatures. There is no clear difference in the spectra of WO_3 films which were annealed at 80 ^{0}C, 160 ^{0}C, 220 ^{0}C and 300 ^{0}C in vacuum. There is also no clear difference in the spectra of WO_3 films annealed in vacuum and air. The films grown at RT were only treated at low temperature (≤300°C). This limitation was caused by the demand of fabrication of the smart windows, ECDs and other functional multi-layer films.

Reflection and roughness (δ). Similarly to Section 7.3.4 Fig. 7-5-3 shows the diffuse reflectance (DR) and specular reflectance (SR) spectra of the annealed WO_3

films. All DR spectra of the WO$_3$ films exhibit similar shape and very low intensity (less than 5.0%). All SR spectra of the WO$_3$ films exhibit similar shape and about 25% average intensity. The δ values, from 3.7-4.9 nm in our samples, were calculated by the TIS method. The AFM observations agree with these results. Fig. 7-5-4 is a typical AFM measurement of the surface microstructure of the film deposited at RT with 70 % P$_{O2}$. A rough surface and nanometer grain boundaries are clearly seen in the figure. The average grain size is ~36 nm, the average height of δ is less than 6 nm. One random bigger grain (~110 nm) appears or does not appear in any one square μm area on the films.
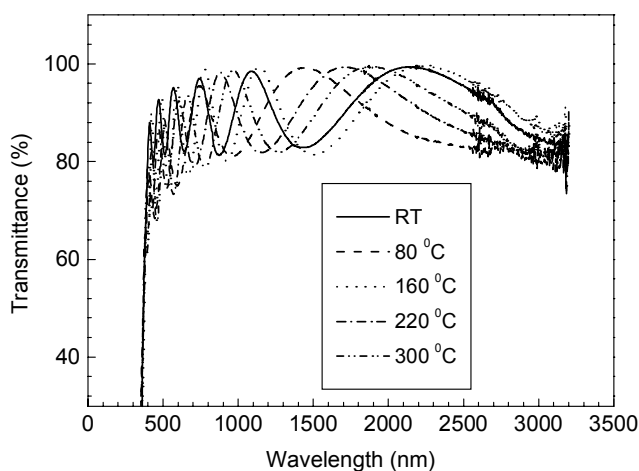

Fig. 7-5-2. Transmittance spectra of WO$_3$ films (sample-W2) deposited at room temperature, -70 V bias, 70% P$_{O2}$, and annealed at different temperatures in vacuum.
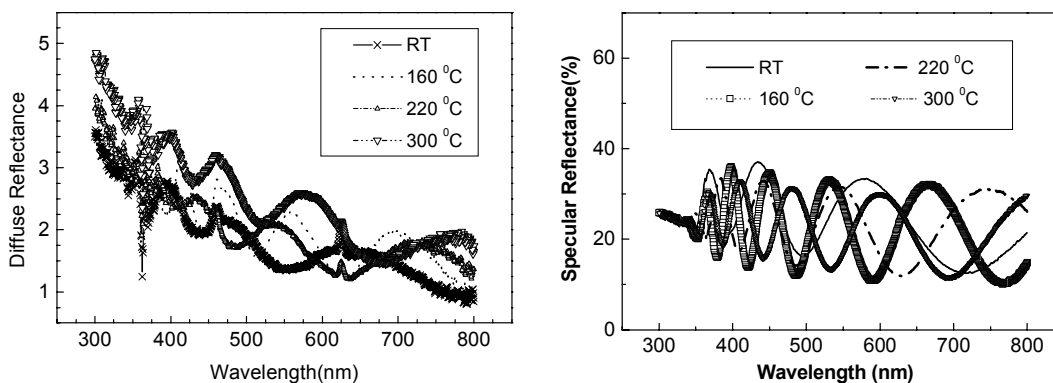

Fig. 7-5-3. The diffuse reflectance (DR) and specular reflectance (SR) of WO$_3$ films deposited at room temperature in -70 V bias in 70% P$_{O2}$ and annealed at different temperatures in vacuum.
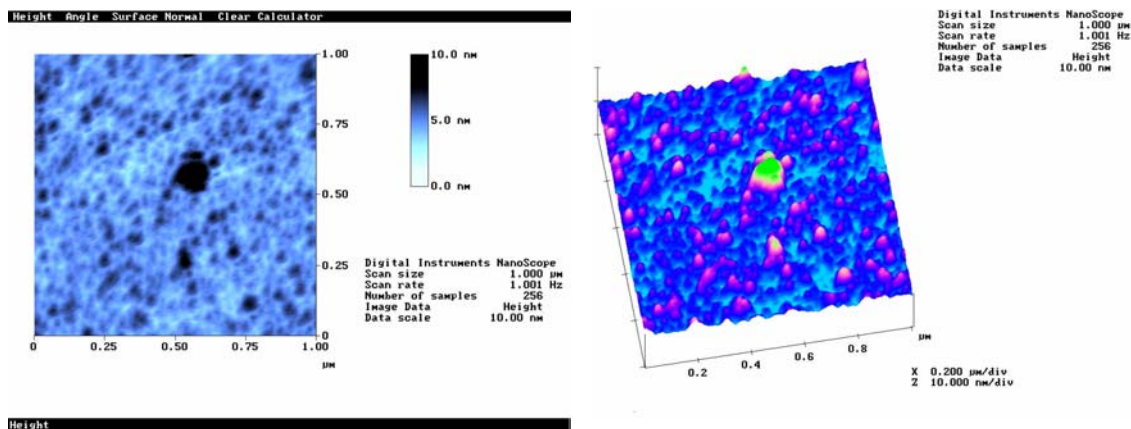
Fig. 7-5-4. AFM topography of a WO$_3$ film deposited with 70% oxygen partial pressure, -70 V bias, and 80 ^{0}C post annealing in vacuum.

7.5.4. Conclusions of the section

The effects of vacuum and air annealing (25°-300°C) on IR absorption and UV-vis-NIR transmittance and reflection of the WO$_3$ films were discussed. The IR spectrum was constituted of broad peaks in the 1453-3600 cm^{-1} region. Those bands are assigned to ν(OH) and δ(OH) modes of adsorbed water. The corresponding tungsten oxide vibrations are in the infrared regions of 1453-400 cm^{-1} and 3506 cm^{-1}, which correspond to tungsten-oxygen stretching, bending and lattice modes. We found some relatively strong and weak bands at 417, 500, 670 (690) and 990 (970) cm^{-1}. The IR investigations of WO$_3$ revealed information about the structure and water molecules with tungsten. The annealing treatment of the films at less than 300 ^{0}C results in no decomposition of the film. The strong peak at 1142 cm^{-1} was assigned to δ(OH) in the W-OH group. The shoulder around 982 cm^{-1} (W=O terminal modes of surface grains) and W-O-W bridging mode 853 cm^{-1} rises after annealing. The 670 cm^{-1} band was tentatively assigned to the out of plane deformation W-OH mode when hydrogen is located at a coplanar square of oxygen atoms. The 500 cm^{-1} band was assigned to the strong coupling of the oxide lattice in hydrated WO$_3\bullet$nH$_2$O material.

There is no clear difference in the transmittance and reflection spectra of WO$_3$ films annealed at 80 ^{0}C, 160 ^{0}C, 220 ^{0}C and 300 ^{0}C in vacuum. There is also no clear difference in the spectra of WO$_3$ films annealed in vacuum and air. All DR spectra of the WO$_3$ films exhibit similar shapes and very low intensity (less than 5.0%). All SR spectra of the WO$_3$ films exhibit similar shapes and about 25% average intensity. The calculated δ value is in the range 3.7-4.9 nm. The average AFM grain size is ~36 nm,

the average height of δ is less than 6 nm except one random bigger grain (~110 nm) that appears in one square μm area on the films.

7.6. Molecular Vibration Spectra of Tungsten Oxide Thin Films

7.6.1. Introduction

There has been many progresses in infrared (IR) and Raman spectrum[38, 43]. However, these were not systematically investigated for one same sample using the two techniques. Especially inorganic compounds such as WO_3 were not studied systematically.

Granqvist had given brief statements about vibrations in the range 400-1200 cm^{-1} [6]. Raman spectrum can detect the structures of the films. The Raman vibration mode is related to the molecular structures by comparison with standard compound spectra or with Raman theoretical calculations. The use of Raman scattering to study thin film has been reported [44, 45]. The accuracy, reliability, and interpretation of the Raman spectra of tungsten oxide catalysts has been discussed [46, 47].

As it is known, the structure and components of the material dominate the properties of thin films. Both IR and Raman spectroscopy are very powerful tools to analyse the structure, phase and components of materials such as tungsten oxides [39, 48, 49]. They are suitable to study the vibration and rotation of molecules. With these techniques, it is possible not only to identify different oxide phases but also to detect intercalated H_2O. The vibration spectroscopies play a key role in the characterization of EC films. Such studies allow obtaining fundamental information about WO_3 films for applications. In this section, an investigation of Raman spectroscopy on tungsten oxide thin films is done, and all the vibration spectrum data, including IR and Raman, is summarized and discussed.

7.6.2. IR and Raman Vibrational spectra of WO_3 thin films

Since inorganic compounds have vibrational bands mainly below 1200 cm^{-1}, an investigation of IR and Raman spectroscopies of WO_3 thin films was done in the range 250~1200 cm^{-1} [43, 38]. Bange [50] has studied vacuum deposited tungsten oxide films by mass spectroscopy. It was observed that the mass spectrum of the films consists of WO_2, WO_3, W_2O_6, W_3O_8 and W_3O_9. The WO_3 structure consists of an infinite number of packed corner-sharing $(WO_6)^{6-}$ octahedra. To elucidate how many clusters are necessary to give the bulk properties, Nagai [30] calculated the electronic structure of the

clusters in various dimensions. Even an accumulation of 12 clusters is not sufficient to represent the bulk properties [12]. In the following section, the observed vibrational spectra are described and discussed.

To consolidate the observations made by the various research groups, values that fall in different frequencies were grouped together for simplicity. This is a reasonable way to present such data since one is dealing with solid-state spectroscopic measurements that show effects due to oxygen stoichiometry variations, crystalline disorder, mixed phases, attainable signal-to-noise ratio, instrument calibration errors and variations in the technique. The assignment and comparison of the characteristic vibrations of the IR (Section 7.5) and Raman spectra are given in Table 7-6-1.

Table 7-6-1. Summary of observed and literature data of the IR and Raman for WO_3

IR(cm^{-1}) Exp.: RT/300 ^{0}C	IR(cm^{-1}) Ref.	IR Groups & Assignment	Raman (cm^{-1}) Exp.: RT/300^{0}C	Raman (cm^{-1}) Ref.	Raman Groups & Assignment
1142/1167	1156[36]	W-OH	990/990	992[65]	$\nu(WO_2)$
990/982	995[41]	ν W-O,			
-	989[63]	$\nu(W_2O_6\&W_3O_8)$	969/974	971[42]	ν_s(W=O ter.)
-	965[41]	ν(W-O)	928/923	928[65, 30]	$\nu_a(WO_2)$
-	925[41]	ν(W-O)	883/883	874 [30]	$\nu(W_3O_9)$
884/853	874	$\nu(W_3O_9)$	842/847	830[66]	W-O-O
-	835[41]	ν(W-O-W)	790/790	790 [51, 30]	ν_a(W-O-W)
-	780, 800[41]	ν(W-O-W)	694/694	694[63]	$\nu(W_2O_6\&W_3O_8)$
670/670	670[41]	γ(W-O-W)		680[67]	Np.
-	660[64]	ν(O-W-O)	503/505	500[36, 39]	O-Lattice
500/515	500[36, 39]	O-Lattice	417/417	418[41]	δ(W-O)
417/417	418[41]	δ(W-O)	318/318	300[35]	$\nu(WO_3)$
-	290[41]	δ(W-O)		330[39] [34]	δ(O-W-O)
-			272/273	270[42]	ν(O-W-O)
-	275 [41]	δ(W-O)		270[34]	δ(O-W-O)
-	-	-	221/221	220[49]	W-W
-	-	-			

Ref.: reference; Exp.: experiment ; ν_s : symmetric stretch; ν_a : anti symmetric stretch; ter.: terminal; Np.: nanocrystalline phase

7.6.3. Raman Assignments of WO_3 structure

The details of the IR assignment of the films were discussed in 7.5 Section. Fig. 7-6-1 shows the Raman spectra of as deposited WO_3 films, prepared at RT, -70 V bias in 70% P_{O2} and annealed at 300 ^{0}C for one hour. Raman spectra of WO_3 films deposited at 300 ^{0}C with different P_{O2} were measured and are shown in Fig. 7-6-2. The 990, 969, 928, 790, 503, 417 and 273 cm^{-1} bands were observed in Raman spectra.

Raman bands of the transition metal (M) oxide in the range 1050 - 950 cm^{-1} can be assigned to a symmetric stretching mode of short terminal M=O bands, ν_s (M=O ter.). The bands in the range 750 - 950 cm^{-1} are attributed to either the antisymmetric stretch of M-O-M bonds (i. e., ν_{as} [M-O-M]) or the symmetric stretch of (-O-M-O-) bonds (i. e., ν_s [-O-M-O-]) [51]. The strongest peak located at 969 cm^{-1} (Fig. 7-6-1) belongs to ν_s (W=O ter.) of cluster boundaries [52]. The W=O terminal stretching belongs to the W-O bonds at the free surface of internal grains. This remarkable relative intensity of the double W=O bond, typical of non bridging oxygen, is caused by the absorbed water molecules and is frequently seen in sputtered or evaporated films deposited at lower temperatures [39].
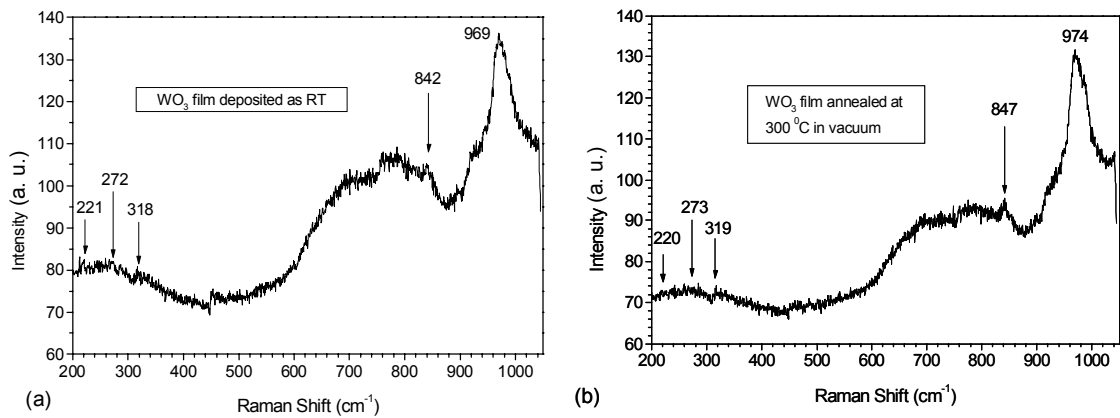

Fig. 7-6-1. Raman spectra of WO$_3$ film deposited at RT and -70 V bias in 70% P$_{O2}$. (a) as-deposited and (b)annealed at 300 ^{0}C for one hour in vacuum.
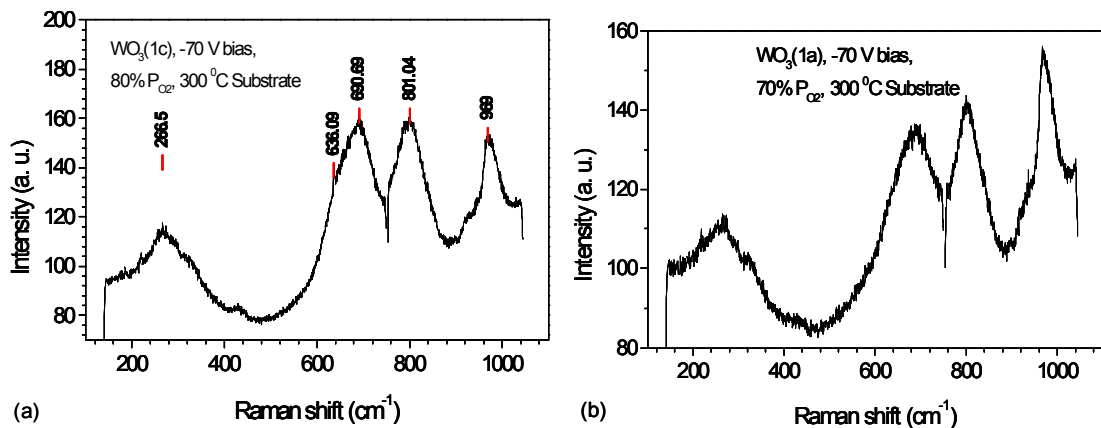

Fig. 7-6-2. Raman spectra of WO$_3$ films deposited at -70 V bias and 300 ^{0}C in (a) 80% P$_{O2}$ (ratio of oxygen partial pressure) and (b) 70% P$_{O2}$.

Fig. 7-6-1 shows a typical Raman spectrum. Before and after annealing the films show a similar Raman curve [9]. Small variations of the intensity between the spectra are found in all the range. All the background from the underlying glass slide in the spectra decreases after annealing of 300 ^{0}C, that is, the I_R/I_N ratio of Raman intensity (I_R) and noisy signal intensity (I_N) increased after annealing.

Since there is no feature corresponding to the peak of 969 cm^{-1} in the Raman spectra of crystalline WO_3 (WO_3 crystal does not have any double bond) [35, 53], all the above facts supports the hypothesis of an open (or porous) structure of the films with many inner empty spaces and inter-grain boundaries. This means that comparably small amounts of water were absorbed in the films. The results suggest that the formation of porous films is due to gas-phase reactions in the plasma, leading to a homogeneous nucleation of oxide particles on the substrate. Clearly the prepared films were not a typical crystalline WO_3 (monoclinic phase or m-phase) structure.

A broad band is observed at 600-900 cm^{-1} in Fig. 7-6-1. The band comes from the combination of the weak peaks 883, 807, 790, 713, 694 and probably includes 645 cm^{-1} too. The peaks at 807 and 713 are typical Raman peaks of crystalline WO_3 (m-phase), which correspondes to the stretching vibrations of the bridging oxygen [16, 54]. These peaks are assigned to W-O stretching (ν), W-O bending (δ) and O-W-O deformation (γ) modes respectively [39, 48, 52, 55]. A. Rougier et al [34] proved the above results. They showed that a rather featureless broad band of deposited WO_3 films in the 600-900 cm^{-1} region split in two sharper peaks located around 715 and 807 cm^{-1} after annealing at 400 ^{0}C. The 645 cm^{-1} peak belongs to the O-W-O mode of $WO_3 \cdot nH_2O$ [52]. The broad asymmetric band at 645 cm^{-1} is probably associated with stretching motions within the equatorial plane and is inside the range of 600-800 cm^{-1}. There is a weak band at 842 cm^{-1}, which can signal the presence of peroxo groups as ν(W-O-O) [54]. All the above discussions indicate that the clusters of the film are connected to each other by W-O-W or hydrogen bonds through water bridges with terminal W=O bonds at the surface of the clusters [56].

Since the W $=$ O double bond is stronger than the W-O single bond, its vibration frequency is expected to be higher than that of the W-O bond. As it is known, there are some difference about the position of the W=O bond (range of 930-975 cm^{-1}) for different references in Table 7-6-1. D. Gazzoli et al [47] indicated that the Raman positions depended on the tungsten content: the higher the W content, the higher the frequency at which the band appears and the removals of water causes a shift of the

Raman bands to higher frequency. There is a difference in our ex-situ Raman spectra before and after heat treatment at 300 ^{0}C. The peak at 969 cm^{-1} shifts to higher frequency (974 cm^{-1}) after annealing. Due to above statements, the 974 cm^{-1} peak indicates that the α-WO$_3$ film presents more oxygen deficiency and the 969 cm^{-1} indicates more moisture on the film before annealing. Since it is an ex-situ measurement, even if we remove the surface water molecules of the film they can be partly absorbed on surface again during the experiment after annealing. Hence we deduced that the shift comes from the internal structure or phase of the film, not from the surface of the film.

In addition probably an increase of compressive residual stress of the film due to annealing causes Raman shift to higher wavenumbers. This phenomenon has also been observed in IrO$_2$ films [57], ZrO$_2$ films [58] and on the GaAs-SiO$_2$ interface [59]. Considering the residual stress and the Raman peak position before and after annealing, it can be concluded that the Raman peak position shifts to higher wavenumbers with the increase of compressive stress and it shifts to lower wavenumbers with the increase of tensile stress. To obtain a quantitative measurement of the residual stress of the WO$_3$ films, more detailed work is needed.

7.6.4. Curve Ftting of Raman Spectrum

Curve fitting (Fig. 7-6-3a) of annealed WO$_3$ film spectrum (Fig. 7-6-1b) was done. It was found that the spectrum of the WO$_3$ film is characterized by as many as 7 modes in the 600 ~ 1000 cm^{-1} region. The approximate position of each mode is shown in Fig. 7-6-3a. Statistical analysis of the peak positions indicate that 7 spectra modes are found at 997 (IR 995, ν $_{W-O}$), 973(Raman 971, ν$_s$(W=O ter.), 921 (IR 925, Raman 923 or W metal), 843 (Raman 842, W-O-O), 789 (Raman 790, ν$_a$ (W-O-W)), 739.8 and 688.1 (Raman 680, Np; 694, ν (W$_2$O$_6$ &W$_3$O$_8$)) cm^{-1}, however 739.8 mode has not been assigned. The band positions in bracket are listed in Table 7-6-1.

Nearly all the fitted peaks agree with assignments of IR or Raman of WO$_3$ presented in the Table. Since IR and Raman spectra on films have special characters already mentioned in Section 7.6.2. The Raman spectra for powders of WO$_3$ and WO$_3$(H$_2$O) are given as a comparison in Fig. 7-6-3 (b). The pure tungsten peak in the 920 cm^{-1} position is a broad band with ~45 cm^{-1} FWHM. Because the bands at 635 and 943 cm^{-1} in Fig. 7-6-3b are assigned to the A$_g$ phonons of the WO$_3$(H$_2$O)$_x$ lattice as observed by other researchers [39, 48, 53], and there are not clearly the two bands in the fitting analysis of the

sample, the post-annealed films are mainly WO_3 (or the absorbed water was sufficiently removed) and are not typical $WO_3(H_2O)_x$ (tungstite). To get the exact amount of absorbed water, more quantitative analysis has to be done.

In the case of tungstite, the unit cell of the orthorhombic crystal consists of four distorted octahedral [60]. One of the axial oxygen positions in the octhedra could occupy by a structural water molecule (Fig. 7-6-3c and Fig. 7-2-2). This oxygen is associated with a much longer single bond than the opposite axial oxygen which forms the W=O double bond (referred to as the terminal bond) and is associated with the 920 cm^{-1} tungsten peak or 943 cm^{-1} mode.

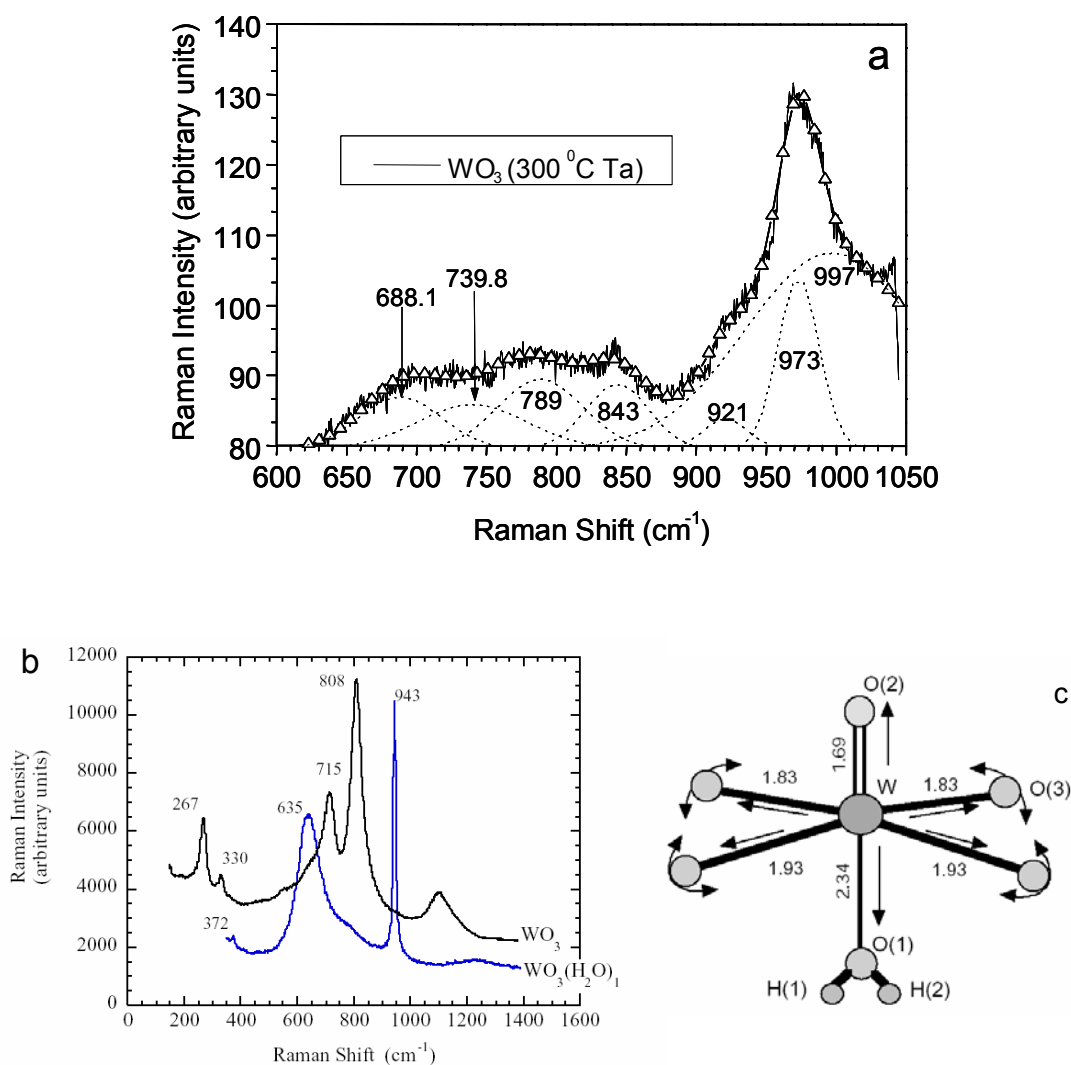**Fig. 7-6-3.** (a) Curve fitting analysis of the Raman spectrum of WO_3 film in the 600 -1000 cm^{-1} region; (b) Raman spectra for powders of WO_3 and $WO_3(H_2O)$; (c) Diagram of one of the octahedra which exists in $WO_3(H_2O)_x$. Approximate bond lengths and some of the many bending and stretching modes which are Raman active are also shown.

The modes at 808 and 715 cm^{-1} in the spectrum have been assigned to the Ag phonons of the WO_3 lattice (Fig.7-6-3b) for WO_3. The unit cell of the WO_3 crystal consists of eight corner sharing distorted and tilted WO_3 octahedra [48, 61]. Literature values for bending or deformation motions of the O-W-O equatorial bonds within the octhedra of crystalline WO_3 are 267 and 330 cm^{-1} [39, 48].

7.6.5. Lower wavenumber Raman

M. Regragui *et al.* [42] reported that they observed the sharp peak at 220 cm^{-1} and other peaks in the range 90-280 cm^{-1}. Obviously there are a group of weak peaks at the range of 200-300 cm^{-1} in the Raman spectra of Fig. 7-6-1 and Fig. 7-6-2. The quantum computations are now an essential part of the most common analytical tools used for materials characterization. Similar vibrations were obtained by Raman theories and are in agreement with the results of De Wijs *et al.* [54]. They studied WO_3 using first-principles calculations and then obtained information on the electronic and spatial structure with high accuracy on the microscopic scale. They conluded that the 220 cm^{-1} peak is originated from W^{5+}-W^{5+} or W-W vibrations [49]. The occurrence of the peak is correlated with the amount of oxygen deficiency. The evidence from the theory agrees with our Raman experiments (210 cm^{-1} weak band). According to previous research, the Raman activity of phonons is caused by the successive deformation of the cubic lattice. Most peaks below 200 cm^{-1} are attributed to lattice modes, whereas the mid and high frequency regions correspond to deformation and stretching modes, respectively. The sharp peaks at 270 and 330 cm^{-1} are assigned to the bending vibration δ(O-W-O) [34, 39]. The Raman peak at 272 cm^{-1} is very weak, which means that a small fraction of crystalline phase presents in the films. The 807, 713 (Section 7.6.3) and 272 cm^{-1} are typical modes of the crystalline WO_3 film. All these peaks are in good agreement with what has been found in WO_3. Comparing our Raman spectra with that of polycrystalline WO_3 and α-WO_3 films [9], our WO_3 film has both polycrystalline WO_3 (in the range 100-300 cm^{-1}) [16, 34, 43, 49, 68] and α-WO_3 (in the range 500-1000 cm^{-1}), but consists mainly of α-WO_3 state.

7.6.6. Raman and IR assignments of other W_xO_y structures

Assignment of other W_xO_y structures such as WO_2, W_3O_9, W_2O_6 and W_3O_8 were done in the following manner.

(i) WO_2 has C_{2v} symmetry structure. As for the vibrational properties of O=W=O, three bands at wavenumbers 300 cm^{-1} (bending), 928 cm^{-1} (v-anti stretch or v_a) and 992 cm^{-1} (v-stretch) were reported in the IR region [30, 65]. The bond angle of O=W=O and bond length of W=O is 110^0 and 0.181 nm. The 300 cm^{-1} mode was observed at very weak 302 cm^{-1} peak of Raman of Fig.7-6-2 (curve a and b). The 928 cm^{-1} mode was observed at weak shoulder peak of Raman (curve b in Fig. 7-6-2). The 992 cm^{-1} mode was observed in 990 cm^{-1} of IR and 990 cm^{-1} weak peak of Raman (Table 7-6-1). The valence of the tungsten atom is 4^+ instead of 6^+ in WO_2. The results show that the prepared WO_3 films, which were deposited at -70 V bias and 300 ^{0}C T_s in 80% and 70% P_{O2}, present a small amount of WO_2.

(ii) The vibrational frequency mode at 694 cm^{-1}, 989 cm^{-1} and 1007 cm^{-1} were observed in the IR region and correspond to W_2O_6 and W_3O_8 [63]. The 694 cm^{-1} weak peak was observed in Raman. The 989 cm^{-1} mode was observed in IR (weak 990 cm^{-1}) and Raman (990 cm^{-1} side peak). It shifts to 982 cm^{-1} (WO_3), after annealing in IR.

(iii) The vibrational frequency modes at 487 cm^{-1}, 874 cm^{-1} and 1024 cm^{-1} were observed in the Raman region, it corresponds to W_3O_9 [62] in IR region. The 487 cm^{-1} mode is from the very weak Raman 488 cm^{-1}. Possibly the observed weak 884 cm^{-1} (853 cm^{-1} after annealing) in IR and weak 883 cm^{-1} in Raman corresponds to the 874 cm^{-1} mode of W_3O_9.

7.6.7. Conclusions of the section

The vibrational spectra including IR and Raman assignments of fundamentals were reported. The Raman spectra are in accordance with IR spectra of WO_3 films before and after annealing. Assignment of the W_xO_y structures, such as WO_2, WO_3, W_3O_9, W_2O_6 and W_3O_8, were discussed. A few mount of W_xO_y structure exists in the prepared WO_3 films.

The strongest Raman peak was located at 969 cm^{-1}, which is assigned to a terminal W=O stretching mode of cluster boundaries. After annealing the Raman peak position shifts to higher wavenumbers (974 cm^{-1}) which can be explained by the two reasons. (1) The 974 cm^{-1} peak indicates that the α-WO_3 films are related with the oxygen deficiency in the films. The WO_3 films have more moisture before annealing. (2) The peak shifts to higher wavenumbers with the increase of compressive stress and it shifts to lower wavenumbers with the increase of tensile stress.

We observed both 690 and 500 cm^{-1} band which has controversy in both IR and Raman spectra. Our IR and Raman spectroscopy investigations of WO$_3$ have revealed important information about the water molecules. The annealing treatment of the films results in no decomposition of the films. Because of the ex-situ IR and Raman measurements, during the operation there are some absorbed water in the films. This is why there are only little differences between RT and annealed in some samples. Further curve fitting analysis was done and confirmed that the prepared films are composed by WO$_3$. It is found that the spectrum of the annealed WO$_3$ film is characterized by as many as 7 modes in the 600 - 1000 cm^{-1} region. Since there are no clearly 635 and 943 cm^{-1} bands, which are assigned to the A$_g$ phonons of the WO$_3$ (H$_2$O)$_x$ lattice, the post annealed films are mainly WO$_3$. The peaks at 210 cm^{-1} and in the range 200 cm^{-1} -300 cm^{-1} (lower wavenumbers) were observed and discussed. Comparing our Raman spectra with that of polycrystalline WO$_3$ and α-WO$_3$ films, our WO$_3$ films have both polycrystalline WO$_3$ (in the range 100-300 cm^{-1}) and α-WO$_3$ (in the range 500-1000 cm^{-1}), but mainly the α-WO$_3$ phase. IR and Raman spectroscopies agree with that of XPS and XRD results in assessing the film structure.

7.7. Summary of the Chapter

Amorphous tungsten oxide (α-WO$_3$) and Mo doped WO$_3$ thin films were deposited on glass and ITO substrates by dc reactive magnetron sputtering. General characteristics and structures of WO$_3$ and of transition metal oxides such as perovskite-like, rutile-like, and tungsten oxide hydrates are introduced and discussed.

We gave detailed discussions and results on the amorphous WO$_3$ films deposited with different P$_{O2}$, bias and substrate temperatures plus low temperature annealing (25°-300°C) in vacuum and air. We obtained the composition and structure information on the WO$_3$ films by the reflection-absorption infrared (IR) technique. The IR spectra were constituted of many broad peaks in the 1453-3600 cm^{-1} region. Those bands were assigned to ν(OH) and δ(OH) modes of adsorbed water. The corresponding tungsten oxide vibrations are in infrared regions of 1453-400 cm^{-1} and 3506 cm^{-1}, which correspond to tungsten-oxygen stretching, bending and lattice modes. The Raman vibrational spectra of tungsten oxide films were also discussed. Both IR and Raman spectra confirmed the vibration bands. The IR and Raman were also used to estimate the effect of post thermal annealing and substrate heating on the structure of the films. The basic features of Raman and IR spectra did not change after annealing up to 300 ^{0}C,

thus indicating that the low temperature annealing of WO_3 doesn't destroy the original structure. Further curve fitting analysis was done, and it confirmed that the prepared films contain WO_3. Assignment of the W_xO_y structures, such as WO_2, WO_3, W_3O_9, W_2O_6 and W_3O_8, were discussed. A few W_xO_y exists in the prepared WO_3 films.

XRD and XPS was used to analyze the material composition, and confirmed that the films are WO_3 or MoO_3 doped WO_3. The results from XPS and XRD agree with the IR as well as with the Raman results. The results on the tungsten oxide films show that for low P_{O2} they present an amorphous WO_3 phase, while for higher P_{O2} than the former, they present a mixture of a more crystalline WO_3 phase and a $W_{20}O_{58}$ ($WO_{2.90}$) phase.

The thin films were analyzed by spectroscopy in the mid infrared, near infrared, visible and ultraviolet spectral regions. The films deposited at both RT and 300 ^{0}C, with different P_{O2}, presented higher transmittance from 95% to 98% T_{max}. It was observed that the E_g value of the films varies from 3.35 to 3.57 eV. From AFM results and TIS calculations the average grain size of the films is less than 36 nm, and the average height of δ is less than 6 nm. One random bigger grain (~110 nm) appears in one square μm area on the films. SEM and AFM studies gave detailed information about the structure and morphology of the WO_3 films.

7.8.   References

[1]   S. K. Deb, Appl. Opt. Suppl. 3 (1969) 192.

[2]   C. Trimble, M. DeVries, J. S. Hale, D. W. Thompson, T. E. Tiwald, J. A. Woolam, Thin Solid Films 355 –356 (1999) 26.

[3]   I. Bedja, S. Hotchandani, R. Carpentier, K. Vinodgopal, P. V. Kamat, Thin Solid Films, 247 (1994) 195.

[4]   A. Monteiro, M. F. Costa, B. Almeida, V. Teixeira, J. Gago, E. Roman, Vacuum, 64 (2002) 287-291.

[5]   C. G. Granqvist, Solar Energy Materials & Solar Cells 60 (2000) 201.

[6]   C. G. Granqvist, Handbook of inorganic Electrochromic Materials, (Elsevier, Amsterdam, 1995).

[7]   M. R. Tubbs, Phys. Status Solidi A 21 (1974) 253

[8]   P. F. Carcia, E. M. McCarron III, Thin Solid Films 155 (1987) 53.

[9]   J. V. Gabrusenoks, P. D. Cikmach, A.R. Lusis, J. J. Kleperis and G. M. Ramans, Electrochromic colour centres in amorphous tungsten trioxide thin film, Solid State Ionics 14(1984)25-30.

[10]   G. M. Ramans, J. V. Gabrusenoks and A. A. Veispals, Phys. Satus Solidi 74a (1982) k41.

[11]   T. C. Arnoldussen, J. Electrochem. Soc. 128 (1981) 117.

[12]   E. Salje, K. Viswanathan, Acta Cryst. A 31 (1975) 356.

[13]   L. E. Depero, S. Groppelli, I. Natali-Sora, L. Sangaletti, G. Sberveglieri, E. Tondello, J. Solid State Chem.,121 (1996) 379.

[14]   L. Seguin, M. Figlarz, A novel supermetastable WO_3 phase, Solid State Ionics, 63-65 (1993) 437-441.

[15]   U. Muller, Inorganic Structural   Chemistry, Wiley, Chichester, 1993.

[16]   P. Tagtstrom, U. Jansson, Chemical Vapour deposition of epitaxial WO_3 films, Thin Solid Films 352 (1999) 107-113.

[17]   T. Nanba, I. Yasui, J. Solid State Chem., 83 (1989) 304-315

[18]   N. Sharma, M. Deepa, P. Varshney, S. A. Agnihotry, FTIR investigations of tungsten oxide electrochromic films derived from organically modified peroxotungstic acid precursors, Thin Solid Films 401 (2001) 45-51.

[19]   M. Herry, J. P. Jolivet and J. Livage, Struct. Bonding 77 (1991) 153.

[20]   B. Gerand, G. Nowogrocki and M. Figlarz, J. Solid State Chem., 38 (1981) 312

[21]   A. Azens, G. Ramans, U. Kanders, A. Levrentyev, Vacuum 43 (1992) 943.

[22]   T. Nanba, S. Takano, I. Yasui, T. Kudo, J. Solid State Chem., 90 (1991) 47.

[23]   V. Teixeira, , A. Monteiro, J. Duarte and A. Portinha ,"Deposition of composite and nanolaminate ceramic coatings by sputtering", Vacuum, Volume 67, Issues 3-4, (2002),p. 477-483.

[24]   Johnson PC. In: Vossen JL, Kern W, editors. Thin film processes II. San Diego: Academic Press 1991.

[25]   H. N. Cui and V. Teixeira, in Y. Zhou, Y. Gu and Z.Li (ed.) Mechanics and Material Engineering for Science and Experiments, Science Press New York Ltd, New York, 2001, p. 292-295

[26]   B. A. Movchan, A. V. Demchishin: Fiz. Metal. Metalloved(Phys. Met. Metallogr). 28 (1969) 653.

[27] S. A. Agnihotry, K. K. Saini, T. K. Saxena, S. Chandra: Thin Solid Films 141 (1986) 183.

[28] K. Nordlund, R. S. Averback , Phys. Rev. B 59 (1999) 20.

[29] http://www.webelements.com/webelements/elements/text/W/radii.html

[30] J. Nagai, Optical and Chemical Properties of Electrochromic Oxide Films for Smart Windows, Electrochim. Acta, 46 (2001) 2049-2053.

[31] C. Cantalini, H. T. Faccio, M. Pelino, Sensors and Actuators B31 (1996) 81.

[32] J. S. Hale, Woollam, Thin Solid Films 339 (1999) 174.

[33] M. G. Hutchins, N. S. Butt, A. J. Topping, J. Gallego, P. Milne, D. Jefrey, I. Brotherston, Electrochimica Acta 46 (2001) 1983.

[34] A. Raougier, F. Portemer, A. Quede, M. EI Marssi, Characterization of pulsed laser deposited WO3 thin films for electrochromic devices, Applied Surface Science 153 (1999) 1-9.

[35] L. Dixit, S. K. Kapoor, I. D. Singh and P. L. Gupta, Indian J. Phys., B51 (1977) 116.

[36] C. J. Wright, J. Solid State Chem. 20 (1977) 89.

[37] G. Atanassor, R. Thielsch, D. Popor, Thin Solid Films 223 (1993) 288.

[38] P. Delichere, P. Falaras, M. Froment, A. Hugot-Le Goff, Thin Solid Films 161 (1988) 35.

[39] F. Daniel, B. Desbat, J. C. Lassegues, B. Gerand, M. Figlarz, J. Solid State Chem. 67 (1987) 235.

[40] M. J. Sienko, H. Oesterreicher, J. Am Chem. Soc. Chem. Commun. 9023 (1968) 6568.

[41] J. Pfeifer, Cao Guifang, P. Tekula-Buxbaum, B. A. Kiss, M. Farkas-Jahnke, and K. Vadasdi, J. Solid State Chem. 119 (1995) 90.

[42] M.Regragui, M. Addou, A. Outzourhi, J. C. Bernede, Elb. EI Idrissi, E. Benseddik, A. Kachouane, Preparation and characterization of pyrolytic spray deposited electrochromic tungsten trioxide films, Thin Solid Films, 358 (2000) 40-45.

[43] H. A. Willis, J. H. van der Maas and R. G. J. Miller, Laboratory Methods in Vibrational Spectroscopy, 3rd Edition, John Wiley & Sons: New York (1987).

[44] B.V. Kolesov, T.V. Basova, I.K. Igumenov, Thin Solid Films, 304 (1997) 166

[45] J.Z. Wan, F.H. pollak, and B.F. Dorfman, J. Appl. Phys., 81 (1997) 6407

[46] Zhao, B.; Xu, X.; Gao, J.; Fu, Q.; Tang, Y. J. Raman Spectrosc. 27 (1996) 549.

[47] D. Gazzoli, M. Valigi, R. Dragone, A. Marucci and G. Mattei, Chara. Of the Zirconia-Supported Tungsten oxide system by Laser Raman and diffuse reflectance spectroscopies, J. Phys. Chem. B 101 (1997) 11129-11135.

[48] E. Salje, Acta Cryst., A 31(1975)360.

[49] S.-H. Lee, Hyeonsik M. Cheong, C. Edwin Tracy, A. Mascarenhas, David K. Benson, Satyen K. Deb, Raman spectroscopic studies of electrochromic a-WO3, Electrochimica Acta 44 (1999) 3111-3115.

[50] K. Bange, Sol. Ener. Mater. And Sol. Cell, 58 (1999) 1.

[51] B. M. Weckhuysen, J.-M. Jehng, I. E. Wachs, In situ Raman Spectroscopy of Supported Transition Metal Oxide Catalysts: $^{18}O_2$-$^{16}O_2$ Isotopic Labeling Studies, J. Phys. Chem. B 2000, 104, 7382-7387.

[52] T. Kubo, Y.Nishikitani, J. Electrochem. Soc. 145(5) (1998) 1729.

[53] M. F. Daniel, B. Desbat, J. C. Lassegues, and R. Garie, Journal of Solid State Chemistry, **73**, 127 (1988).

[54] G. A. de Wijs, R. A. de Groot, Amorphous WO3 : a first-principles approach, Electrochimica Acta 46 (2001) 1989-1993.

[55] A. Anderson, Spectrosc. Lett. 9 (1976) 809.

[56] Y. Shigesato, Y. Hayashi, A. Masui, T. Haranou, Jpn. J. Appl. Phys. 30(4) (1991) 814.

[57] P. C. Liao, C. S. Chen, W. S. Ho, Y. S. Huang, and K. K. Tiong, Thin Solid Films, 301 (1997) 7

[58] A. Portinha, V.Teixeira, J. Carneiro, M.F. Costa, N.P. Barradas and A.D. Sequeira, "Stabilization of ZrO_2 PVD coatings with Gd_2O_3", Surface and Coatings Technology, 188-189 (2004), 107-115.

[59] A. B. M. H. Rashid, M. Kishi, and T. Katoda, J. Appl. Phys., 80 (1996) 3540

[60] J. T. Szymanski and A. C. Roberts, Canadian Minerologist, **22**, 681 (1984).

[61] B. O. Loopstra and P. Boldrini, Acta Crystallography, **21**, 158 (1966).

[62] I. Hargittai, M. Hargittai, V. P. Spiridonov and E. V. Erokhin, J. Mol. Struct. 8 (1971) 31.

[63] W. Weltner and D. McLeod, J. Mol. Spectry., 17 (1965) 276

[64] M. Gotic, M. Ivanda, S. Popovic, S. Music, Synthesis of tungsten trioxide hydrates and their structural properties, Materials Science and Engineering B77 (2000) 193-201.

[65] M. J. Yoder, J. Quant. Spectrosc. Radiat. Transfer., 14 (1974) 1317

[66] U. Opara Krasovec, A. Surca Vuk, B. Orel, IR Spectroscopic studies of charged-discharged crystalline WO3 films, Electrochimica Acta 46 (2001) 1921-1929.

[67] E. Cazzanelli, L. Papalino, A. Pennisi, F. Simone, Spatial variation of structural order in sputtered WO3 films, Electrochimica Acta 46 (2001) 1937-1944.

[68] J. Gabrusenoks, A. Veispals, A. von Czarnowski, K.-H. Meiwes-Broer, Infrared and Raman spectroscopy of WO3 and CdWO4, Electrochimica Acta 46 (2001) 2229-2231.

[69] J.A.Venable, Phil. Mag., 27 (1973) 697

[70] H., J. Reiss, Appl. Phys., 39 (1968) 5045